



TALLINN UNIVERSITY OF TECHNOLOGY

SCHOOL OF ENGINEERING

Department of Electrical Power Engineering and Mechatronics

**ADDITIVELY MANUFACTURED SOLUTIONS WITH  
OPTIMIZED TOPOLOGIES FOR ELECTRICAL  
MACHINE THERMAL APPLICATIONS**

**3D-PRINDITUD OPTIMEERITUD TOPOLOOGIAGA  
JAHUTI ELEKTRIMASINALE**

MASTER THESIS

Student: Alexandre Martí Valero

Student code: 224453MAHM

Supervisor: Martin Sarap, Early Sage Researcher

Tallinn 2024

## **AUTHOR'S DECLARATION**

Hereby I declare, that I have written this thesis independently.

No academic degree has been applied for based on this material. All works, major viewpoints and data of the other authors used in this thesis have been referenced.

"13" May 2024

Author: Alexnadre Martí Valero

*/signature /*

Thesis is in accordance with terms and requirements

"13" May 2024

Supervisor: Martin Sarap

*/signature/*

Accepted for defence

".....".....2024

Chairman of theses defence commission: .....

*/name and signature/*

## **Non-exclusive licence for reproduction and publication of a graduation thesis<sup>1</sup>**

I, Alexandre Martí Valero

1. grant Tallinn University of Technology free licence (non-exclusive licence) for my thesis "Additively Manufactured Solutions with Optimized Topologies for Electrical Machine Thermal Applications",

supervised by Martin Sarap,

1.1 to be reproduced for the purposes of preservation and electronic publication of the graduation thesis, incl. to be entered in the digital collection of the library of Tallinn University of Technology until expiry of the term of copyright;

1.2 to be published via the web of Tallinn University of Technology, incl. to be entered in the digital collection of the library of Tallinn University of Technology until expiry of the term of copyright.

2. I am aware that the author also retains the rights specified in clause 1 of the non-exclusive licence.

3. I confirm that granting the non-exclusive licence does not infringe other persons' intellectual property rights, the rights arising from the Personal Data Protection Act or rights arising from other legislation.

13. May 2024

---

<sup>1</sup> *The non-exclusive licence is not valid during the validity of access restriction indicated in the student's application for restriction on access to the graduation thesis that has been signed by the school's dean, except in case of the university's right to reproduce the thesis for preservation purposes only. If a graduation thesis is based on the joint creative activity of two or more persons and the co-author(s) has/have not granted, by the set deadline, the student defending his/her graduation thesis consent to reproduce and publish the graduation thesis in compliance with clauses 1.1 and 1.2 of the non-exclusive licence, the non-exclusive license shall not be valid for the period.*

## ABSTRACT

Author: Alexandre Martí Valero

Type of the work: Master Thesis

Title: Additively Manufactured Solutions with Optimized Topologies for Electrical Machine Thermal Applications

Date: 13.05.2024

University: Tallinn University of Technology

School: School of Engineering

Department: Department of Electrical Power Engineering and Mechatronics

Supervisor of the thesis: Martin Sarap

Abstract:

High operational temperature in electrical machines incurs in reduced reliability and increase in losses that limits the power density of these machines. Through thermal management these problems can be mitigated. The advent of additive manufacturing allows for the application of Topology Optimization to produce highly complex designs. Therefore, the application of Topology optimization to the design of a water jacket cooling system intends to provide a solution that outperforms current available designs and can improve the thermal management of electrical machines, which in turn will allow for increased power density and reliabilities.

Keywords: Electrical Machines, Topology Optimization, Additive Manufacturing, Water Jacket

## LÕPUTÖÖ LÜHIKOKKUVÕTE

Autor: Alexandre Martí Valero

Lõputöö liik: Magistritöö

Töö pealkiri: 3d-printitud optimeeritud topoloogiaga jahuti elektrimasinale

Kuupäev: 13.05.2024

Ülikool: Tallinna Tehnikaülikool

Teaduskond: Inseneriteaduskond

Instituut: Elektroenergeetika ja mehhatroonika instituut

Töö juhendaja(d): Martin Sarap

Sisu kirjeldus:

Kõrge temperatuur elektriseadmetes põhjustab töökindluse vähenemist ja kadude suurenemist, mis piirab nende seadmete võimsustihedust. Soojuse ohjeldamise abil saab neid probleeme leevendada. Kihtlisandusmeetodi ehk 3D-printimise abil on võimalik rakendada topoloogiaoptimeerimist väga keerukate kujundite tootmiseks. Seetõttu suudab vedelikumantlil põhineva elektrimootori jahutussüsteemi kujunduse topoloogiaoptimeerimine pakkuda lahendust, mis ületab oma jahutusvõimekuselt saadaolevad lahendused, mis omakorda võimaldab suurendada mootorite võimsustihedust ja töökindlust.

Märksõnad: Elektrimasinad, topoloogia optimeerimine, lisaainete tootmine, Veejope

## THESIS TASK

**Student:** Alexandre Martí Valero, 224453MAHM

**Study programme:** MAHM31, Mechatronics Masters

**main speciality:**

**Supervisor(s):** Martin Sarap, Early Satge Researcher

**Consultants:**

**Thesis topic:**

The aim of this thesis work is to design a water jacket cooling system to improve the performance of electric machines. The design is undertaken using topology optimization to maximize cooling efficiency and taking into consideration the manufacturing improvements offered by additive manufacturing.

Käesoleva lõputöö eesmärk on projekteerida veemantli jahutussüsteem, et parandada elektrimasinate jõudlust. Projekteerimisel kasutatakse topoloogia optimeerimist, et maksimeerida jahutuse tõhusust, ning võetakse arvesse lisatootmise poolt pakutavaid tootmisparandusi.

**Thesis main objectives:**

1. Apply Topology Optimization techniques for the realization of a water jacket heat exchanger for and electric motor for later additive manufacturing.
2. Realize different iterations for different proportions of material and starting parameters to find the best possible design.
3. Compare the performance of the design realized and draw conclusions for future work and improvements necessary.

**Thesis tasks and time schedule:**

No	Task description	Deadline
1.	Research on the topic and literature review	February 2024
2.	Familiarization with the software used and definition of the problem	February 2024
3.	Writing of literature review	March 2024
4.	Work to define the CAD designs	March 2024
5.	Testing of different designs	April 2024
6.	Comparison with other current designs	April 2024
7.	Writing of methods and conclusions	May 2024

**Language:** English **Deadline for submission of thesis:** "13" May 2024

**Student:** Alexandre Martí Valero "13" May 2024

*/signature/*

**Supervisor:** Martin Sarap "13" May 2024

*/signature/*

**Head of study programme:** ..... ".....".....20.....a

*/signature/*

*Terms of thesis closed defence and/or restricted access conditions to be formulated on the reverse side*

# Contents

<b>1 INTRODUCTION</b>	<b>11</b>
<b>2 LITERATURE REVIEW</b>	<b>12</b>
2.1 Thermal management of electrical machines	12
2.1.1 Machine cooling objective	12
2.1.2 Air and Liquid cooling	13
2.2 Liquid cooling application in electric machines	14
2.2.1 State of the art of liquid cooling in electric motors	14
2.3 Additive Manufacturing	16
2.3.1 Metal Additive Manufacturing technologies	16
2.3.2 Industrial applications of metal Additive Manufacturing	18
2.4 AM produced Thermal Management Solutions for Electric Machines	19
2.4.1 Air cooling	19
2.4.2 Liquid Cooling	21
2.5 Topology Optimization for heat exchangers	23
2.5.1 Design parametrization	23
2.5.2 Heat Transfer Modelling	24
2.5.3 Optimization	26
2.6 Topology Optimization in COMSOL	27
2.6.1 Optimization algorithms	27
2.6.2 Optimization Theory	29
2.6.3 Topology Optimization	30
<b>3 TOPOLOGY OPTIMIZED DESIGN</b>	<b>32</b>
3.1 Optimization of the desired geometry	32
3.1.1 Heat Conduction Problem	33
3.1.2 Fluid Flow Problem	39
3.1.3 Multi-physics Problem	42
3.1.4 Results with different initial gamma values	49
<b>4 COMPARISON OF SELECTED DESIGN WITH TRADITIONAL SOLUTIONS</b>	<b>53</b>
4.1 Traditional solutions models	53
4.2 Proposed solution model	53
4.2.1 Testing parameters	54
4.2.2 Results for the spiral design	54
4.2.3 Results for the coaxial design	56
4.2.4 Results for the U-shaped design	57
4.2.5 Results for the topology optimized design	58
4.3 Conclusions of the comparison	60
<b>5 SUMMARY</b>	<b>62</b>
<b>6 KOKKUVÕTE</b>	<b>64</b>

## List of Figures

1	Efficiency curves depending on temperature for 7 different electrical machines [5] . . . . .	12
2	Induced air cooling of an electric motor [5] . . . . .	13
3	Liquid cooling scheme where circulation and spray of coolant systems can be observed. Note the rest of the cooling system elements included in the figure [5] . . . . .	15
4	(a) Casting of the cooling jacket, (b) Processed casting with finished machines holes and finished surfaces where and input or output for coolant can be located [8] . . . . .	15
5	(a) Fuel nozzle produced by GE Aviation for LEAP engine. Image credit: GE Additive,(b) Wing bracket of A350 XWB printed with Concept Laser machine and designed by Airbus. Image credit: Airbus Operations . . .	18
6	Topology optimized shape manufactured for comparison against other geometries [46] . . . . .	20
7	Heat exchanger as the motor core in the solar powered aircraft of study [51] . . . . .	21
8	Left: Distribution of spherical and teardrop-shaped dimples on the fin surface. Right: Comparison of thermal performance of the two dimple designs using an overall thermal performance parameter in the Y axis and the Reynolds number of the flow in the X axis [52] . . . . .	21
9	Two side views of the water jacket developed by the NCAM where ribs indicating the presence of cooling channels can be observed [53] . . . .	22
10	(a): Cooling jacket developed by EPMA [54]; (b): Diabatix solution for optimized electric motor cooling jacket [55] . . . . .	22
11	Design domain defined by two variables ( $\chi_1, \chi_2$ ) where infeasible design space represents the limits established by the constraints (red) and the optimum solution is presented in the top of the curve while the initial design starts at lower in the curve, representing a non optimal solution .	28
12	Design domain (50 x 252 mm) with auxiliary geometries (5 x 10 mm) .	32
13	For $V_{target} = 0,5$ . (a): Material distribution inside the domain. (b): Temperature map for material distribution in (a) . . . . .	35
14	For $V_{target} = 0,5$ . (a): Velocity of the fluid inside the domain. (b): Vectors of direction for flow indifferent parts of the design domain. With the data offered in both figures, the path and velocity of the liquid inside the domain can be distinguished . . . . .	36
15	For $V_{target} = 0,4$ . (a): Material distribution inside the domain. (b): Temperature map for material distribution in (a) . . . . .	36
16	For $V_{target} = 0,4$ . (a): Velocity of the fluid inside the domain. (b): Vectors of direction for flow indifferent parts of the design domain. With the data offered in both figures, the path and velocity of the liquid inside the domain can be distinguished . . . . .	37

17	For $V_{target} = 0,3$ . (a): Material distribution inside the domain. (b): Temperature map for material distribution in (a) . . . . .	37
18	For $V_{target} = 0,3$ . (a): Velocity of the fluid inside the domain. (b): Vectors of direction for flow indifferent parts of the design domain. With the data offered in both figures, the path and velocity of the liquid inside the domain can be distinguished . . . . .	38
19	Topology optimization result of the Fluid flow problem . . . . .	41
20	(a): Velocity field showing the regions of the geometry with circulating flow; (b): Color gradient plot of velocity magnitude showing the velocity value of the flow inside the domain . . . . .	41
21	Pressure map of the design domain . . . . .	42
22	Topology optimization results of material distribution . . . . .	44
23	Domain temperature maps for volumetric factor of 0,3: (a) $A_1$ , (b) $A_2$ . . . . .	45
24	Domain pressure maps for volumetric factor of 0,3: (a) $A_1$ , (b) $A_2$ . . . . .	46
25	Flow velocity in the domain for volumetric factor of 0,3: (a) $A_1$ , (b) $A_2$ . . . . .	46
26	Domain temperature maps for volumetric factor of 0,5: (a) $A_1$ , (b) $A_2$ . . . . .	47
27	Domain pressure maps for volumetric factor of 0,5: (a) $A_1$ , (b) $A_2$ . . . . .	48
28	Flow velocity in the domain for volumetric factor of 0,5: (a) $A_1$ , (b) $A_2$ . . . . .	48
29	Material distribution for: (a) $\gamma_i = 0,3$ ; (b) $\gamma_i = 0,5$ ; (c) $\gamma_i = 0,7$ ; (d) $\gamma_i = 1$ ; . . . . .	50
30	Domain temperatures for: (a) $\gamma_i = 0,3$ ; (b) $\gamma_i = 0,5$ ; (c) $\gamma_i = 0,7$ ; (d) $\gamma_i = 1$ ; . . . . .	51
31	Absolute velocities inside the domain for: (a) $\gamma_i = 0,3$ ; (b) $\gamma_i = 0,5$ ; (c) $\gamma_i = 0,7$ ; (d) $\gamma_i = 1$ ; . . . . .	52
32	Traditional water jacket designs: (a)Spiral, (b)U-shaped, (c)Coaxial [91] . . . . .	53
33	3D model of selected result: (a) Model of the result on the interior of the water jacket; (b): Water jacket model exterior showing input and output ports . . . . .	54
34	Spiral design: (a) Water jacket temperature, (b) Cross section of water jacket . . . . .	55
35	Speed of the flow inside the channels for the spiral deign . . . . .	55
36	Coaxial design: (a) Water jacket temperature, (b) Cross section of water jacket . . . . .	56
37	Speed of the flow inside cooling channels of the coaxial water jacket . . . . .	57
38	U-shaped design: (a) Water jacket temperature, (b) Cross section of water jacket . . . . .	57
39	Speed of the flow inside cooling channels of the U-shaped water jacket . . . . .	58
40	TO design: (a) Water jacket temperature, (b) Cross section of water jacket . . . . .	59
41	Speed of the flow inside cooling channels of the TO water jacket . . . . .	59

## List of abbreviations and symbols

**Acronyms and abbreviations** AM - Additive Manufacturing

CV - Control Volume

DED - Directed Energy Deposition

GCMMA - Generalized Convex Approximation Method of Moving Asymptotes

HE - Heat Exchanger

MMA - Method of Moving Asymptotes

SIMP - Solid Isotropic Material with Penalization

SLP - Sequential Linear Programming

SQP - Sequential Quadratic Programming

TO - Topology Optimization

**Symbols**  $\alpha$  - Inverse permeability

$\alpha_r$  - Temperature coefficient for material resistivity

$F$  - Brinkman friction

$G_0$  - Function that ensures that the surface of material generated is smaller than the domain area

$G_i$  - Representation of other constraints

$J$  - Objective function

$k$  - Thermal conductivity [W/mK]

$k_\gamma$  - Thermal conductivity dependent on  $\gamma$  [W/mK]

$M, N$  - Finite elements

$p, p_{in}, p_{out}$  - Pressure [Pa]

$p_{simp}$  - Penalization parameter

$\nabla p$  - Pressure differential [Pa]

$\nabla T$  - Temperature differential [K]

$\Omega$  - Design domain

$p_{fl}$  - Density of a fluid [kg/m<sup>3</sup>]

$\rho_0$  - Material resistivity at ambient temperature [ $\Omega\text{m}$ ]

$\rho_t$  - Material resistivity at given temperature [ $\Omega\text{m}$ ]

$T$  - Working temperature [K]

$T_O$  - Ambient temperature [K]

$u$  - Flow speed [m/s]

$V_{target}$  - Volumetric factor

$\gamma$  - Optimization variable of the optimization problem

$\gamma_p$  - Penalization parameter

$Q$  - Volumetric heat generation [W/m<sup>3</sup>]

# 1. INTRODUCTION

Thermal management of electric machines is crucial to ensure reliable and efficient function of these machines. For instance, the majority of losses originates from the increased resistivity of the copper when it heats up, leading to greater losses with incur in higher inefficiencies, while these high temperatures also lead to the reduction or loss of the magnetic properties of magnets and the rapid degradation of insulator materials in the core.

To ensure the thermal management of these kinds of machines, various cooling solutions exist. On the first place, air cooling can be divided into passive or active air cooling. Passive air cooling makes use of the natural convection phenomenon to exchange thermal energy between the electric machine and the medium, this method relies heavily on the available surface for heat exchange. To enhance the convection, active air cooling makes use of fans to induce greater flow of air and increase the convection and therefore achieve greater heat flux without having to increase the surface area of the heat exchange. Finally liquid cooling, among others techniques, makes use of a water jacket to make water circulate around the stator of the electric machine to extract heat and later exchange it with another medium through a radiator. Because of the higher thermal conductivity of these fluids, a more efficient heat exchange allow for better thermal management.

However, the advent of metal AM with its ability to produce geometrically complex designs, has opened the door to the application of mathematical solutions, like Topology Optimization to engineering design. TO uses mathematical methods to optimize material layout for a defined design domain. TO uses objective and objective function for which it intends to find a maximum or minimum values while obeying the constraints given. Topology optimization has limited applied to thermodynamic applications such as heat exchangers. Therefore, a design of a water jacket for the cooling of an electric machine is realized using Topology optimization, in a 2D space to avoid resource intensive 3D modelling, to achieve a design that allows for better cooling of the motor and therefore allows to increase efficiency, reliability and power density.

Once a design has been defined, a 3D model is composed and compared to three traditional water jacket designs to assess if the achieved design is more effective or less effective than the current solutions. At the end a summary of future work and lessons learned aims to set the base for future manufacturing using metal AM.

**Keywords:** metal AM, Topology optimization, Electric machine cooling

## 2. LITERATURE REVIEW

### 2.1 Thermal management of electrical machines

#### 2.1.1 Machine cooling objective

Thermal management of electrical machines is crucial to maintain and increase both reliability and performance. In the case of electrical machines high temperatures can result in increased conductor resistance, also known as copper losses; and therefore higher losses as well as partially reducing or completely demagnetizing the permanent magnets [1], reducing efficiency (figure 1). Furthermore, higher temperatures have been associated with thermal insulation degradation, with an increase of 10° C in temperature halving the life expectancy of the electrical machine [2, 3], reducing reliability. The loss of efficiency of an electric motor incurs in a loss of power. However the power output of an electric motor is directly proportional to the dimensions is both size and weight. Leading to, the bigger the motor, the powerful it will be, and more heat will be generated and needed to be evacuated. This represents a technical hurdle that limits the power density of electrical machines, and doesn't allow the development of small size and high power motors demanded by the concepts that allow sustainable use of energy [4].

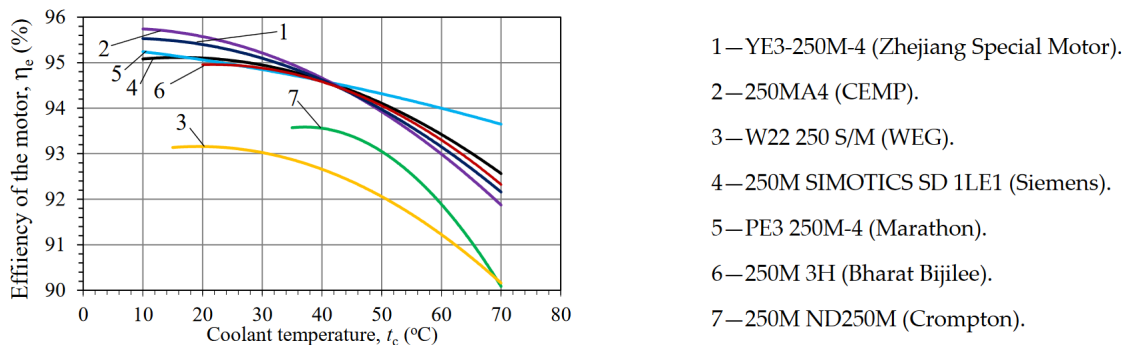


Figure 1: Efficiency curves depending on temperature for 7 different electrical machines [5]

To realise an electric motor with a higher power density, an appropriate cooling solution that allows high temperature evacuation must be applied to allow the motor to function at a high power state without incurring in a loss of reliability and efficiency [6].

#### Copper losses

Copper losses increase in conjunction of conductor resistivity. The resistivity of the conductor, usually copper hence the name, is directly related to the temperature through the following equation:

$$\rho_T = \rho_0[1 + \alpha(T - T_0)] \quad (2.1)$$

Where  $\rho_T$  and  $\rho_0$  represent resistivity at working temperature and initial temperature respectively,  $T$  is working temperature and  $T_0$  is initial temperature and  $\alpha_r$  represent the temperature coefficient.

## 2.1.2 Air and Liquid cooling

### Air cooling

Air dominates as the cooling medium due to its simplicity, cost-effectiveness, and widespread application [7]. Thermal management strategies encompass both interior and exterior motor components to enhance heat exchange area, employing elements like external fins, air circulation ducts, air gaps, and internal/external fan impellers [8].

External cooling mainly utilizes forced convection through a fan on the rotor shaft or an independently actuated fan, points 2 and 10 in figure 2; resulting in an uneven temperature distribution within the electric motor. A better design and the optimization of fan performance and fin geometry can significantly boost cooling system efficiency by 10-30% [9]. And axial designs, have proved more effective than radial designs, becoming the most extended solution [10].

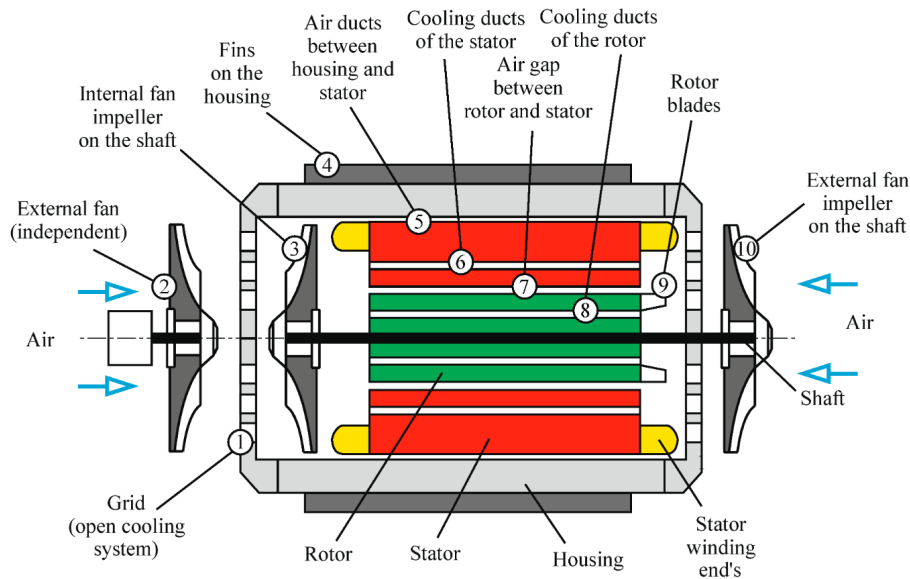


Figure 2: Induced air cooling of an electric motor [5]

Internal air circulation, facilitated by blades on the rotor or shaft impellers, is common in closed electric motors, cooling critical components like stator and rotor windings [11]. Recent research emphasizes internal cooling intensification, incorporating ducts in rotor and stator structures, as shown in points 6 and 8 of figure 2 to reduce working temperatures, enhance operating reliability, and prolong service life [12]. These internal airflow channels improve ventilation efficiency, allowing a reduction in external airflow while maintaining optimized airflow in guide channels, resulting in lower fan noise levels.

For high-power motors, a combination of air cooling methods is common. This technology incorporates primary and secondary circuits, utilizing external fan impellers for forced convection and radiation in the primary circuit, and an internal circuit consisting of a rotor with vent holes and ventilating ducts in the stator housing for additional cooling [13]. Again, a clear example of this case is observed in figure 2, where the diagram of the motor includes: in point 4, external cooling fins; with and an outer fan that forces circulation through them, point 2; and an internal fan, point 3; which circulates air through the ducts present in both the stator and the rotor, points 6 and 8 respectively.

### **Liquid Cooling**

Liquid cooling systems are characterized by the circulation of a liquid through one or more of the components of the motor and then through an external heat exchanger to evacuate the heat extracted from the machine to the ambient. These systems are versatile with the design of the heat exchanger being dependent on the motor's application area and size. Liquid cooling, specially in electric machines is developed in the coming section: section 2.2.

## **2.2 Liquid cooling application in electric machines**

As previously mentioned, liquid cooling systems make use of a liquid that absorbs heat generated, in this case an electric motor. The main system used relies on a liquid coolant that absorbs the thermal energy in the motor and transports it outside to be evacuated through the use of a heat exchanger to another medium. The cooled liquid coolant is recirculated again into the motor, thanks to a closed circuit, to absorb more heat (figure 3). Another solution system relies on the spraying of a cooling solution over materials of the motor, mainly the winding as they are the main source of heat generation on electric motors [14, 15], to absorb the heat generated, the heated coolant is collected in sump and circulated through an heat exchanger to reduce its temperature in order to be used again [13]. Both systems are clearly represented in the schematic in figure 3

### **2.2.1 State of the art of liquid cooling in electric motors**

For the appropriate thermal management of an electrical motor, it is necessary to incorporate a complex system of ducts, channels on the various motor elements. The housing jacket, also known in this case as a "water jacket," is the most common and straightforward liquid cooling method, and can be observed in figure 4 [16]. Typically constructed from various alloys, being aluminum is the most extensively used [16], the housing jacket features liquid distribution facilitated by axial or tangential cooling ducts [8, 17].

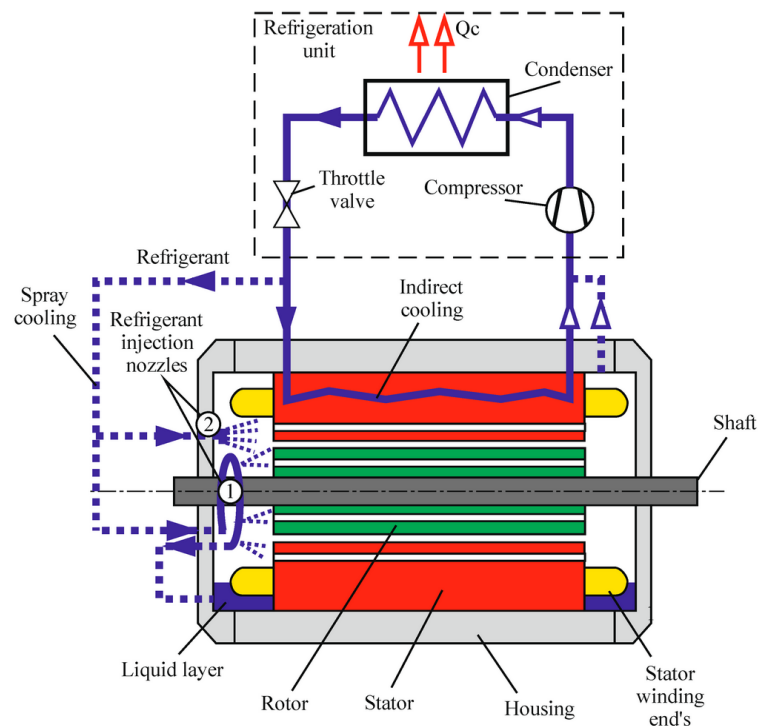


Figure 3: Liquid cooling scheme where circulation and spray of coolant systems can be observed. Note the rest of the cooling system elements included in the figure [5]

Although more effective in reducing motor temperature, the axial ducts present higher hydraulic losses, creating a pressure drop, and therefore exert a higher load on the circulation pump [18]. Resulting in an increased hydraulic resistance in axial channels on the range of 10–15% higher, therefore requiring a more powerful pump. Careful determination of cooling duct geometric characteristics is crucial in optimizing heat evacuation from the motor and hence performance [19, 20].

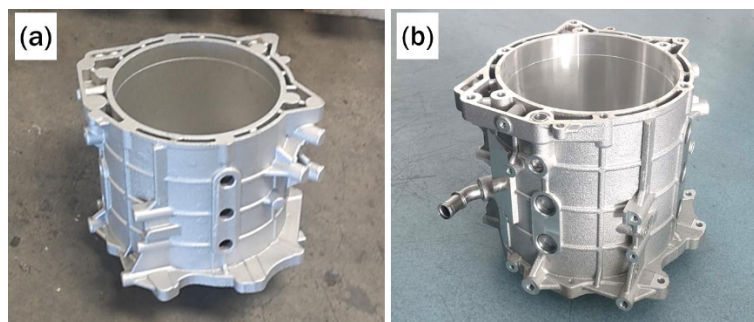


Figure 4: (a) Casting of the cooling jacket, (b) Processed casting with finished machines holes and finished surfaces where and input or output for coolant can be located [8]

The main advantage offered by water jacket cooling systems is a reduced dependence on power load and shaft velocity, since the cooling system pump can function independently of the electric machine. This is an advantage since it ensures a more consistent and higher performance across a wider operational range. For instance, experts have demonstrated a circular water cooling system that reduces stator winding temperature by 13 °C, consequently increasing the power density thanks to reduced losses[21]. A study has explored replacing the housing ducts with tubes in electric motor. Heat

exchange tubes, with diameters ranging from 4 to 8 mm, increase the power density by 2,76 times while maintaining a standard operating temperature. Capillary tubes inside the jacket were also considered, resulting in a 15,5% reduction in temperature for a 1.1 kW three-phase induction motor [22].

## **2.3 Additive Manufacturing**

Additive manufacturing (AM), commonly known as 3D printing, is an emerging manufacturing technology that allows the realization of extremely complex 3D designs realized. For the manufacturing of these complex geometries, AM technology relies on the deposition of material in successive layers until the full geometry is realized [23].

Although now longer in technology demonstration or prototype phase, additive manufacturing is not still widely adopted for full scale manufacturing. Highly specialized industrial sectors such as: aerospace, medical engineering, defense and electronics; have started applying this technology to the production of different components. A more wide application thought more sectors is found in the research and prototyping fields, because of the ease of application of design changes in a new iteration of a prototype due to the fast and cheap manufacturing capacity. If the main advantage of AM is the production of complex geometrical structures not previously capable with conventional manufacturing techniques, and other exposed advantages mentioned are the ease of application of design changes and the capacity to allow for cheap manufacturing of prototypes. Another notable advantages worth mentioning include the reduction of waste material compared to traditional manufacturing techniques [24, 25].

### **2.3.1 Metal Additive Manufacturing technologies**

As of today, AM processes fall into seven categories, and the same applies to metallic AM. The categories are: VAT photopolymerization, material extrusion, material jetting, binder jetting, powder bed fusion, direct energy deposition, and sheet lamination.

#### **Powder Bed Fusion (PBF)**

As of 2020, metal additive manufacturing market is dominated by powder bed fusion (PBF) processes, such as: Direct Metal Laser Sintering (DMLS), Selective Laser Melting (SLM), Electron Beam Melting (EBM), and Direct Metal Laser Melting (DMLM). SLM (or Laser Metal Fusion) and DMLS stand out as they can achieve a superior surface finish and reduced porosity thanks to the ability to produce finer metal layers and a more uniform melt pool [26].

### **Material Extrusion (ME)**

Fused Filament Fabrication (FFF) uses metal milled polymer filaments. The resulting product is not entirely made of metal, but composed of a polymer matrix with metal inserts. Therefore the properties of the printed material change depending on the proportion of metal to polymer [27, 28]. More recently, Bound Power Extrusion (BPE) allows to acquire a metal part with barely polymer content through post processing.

### **VAT Photopolymerization**

This technology only allows to produce metal containing parts through the use of metal infused composite resins [29].

### **Material jetting (MJ)**

In MJ, a photo-polymer resin droplets are sprayed in a precise location and UV light is used to cure and solidify the material. Once a layer is printed, the platform moves down, and a new layer is deposited upon the previous layer until the part is completely built. The resin used is composed of metal powder alongside a liquid binder [30].

### **Binder Jetting (BJ)**

Similarly to MJ, Binder Jetting uses a liquid binder resin infused with metal powder over a moving platform. However, in BJ the metal powder in the droplets is consolidated within and between the layers at room temperature. This technology also works without support structures and allows more accurate printing than other methods [30].

### **Sheet Lamination (SL)**

To build the desired component sheets of material supplied from a feed roller are bonded layer after layer on a platform that moves up and down. Each sheet is cut to the shape with a laser to fit to the part's cross-section. In the most commonly used metal printing method, Ultrasonic Additive Manufacturing (UAM), metallic sheets are bound together using an ultrasonic welding operation [31].

### **Directed Energy Deposition (DED)**

Methods inside DED technology can be grouped into two main categories from an energy perspective: cold spray and thermal energy. Cold spray, sprays fine particles of material to a substrate with enough speed to create a dense layer [32]. The other DED category of methods makes use of a laser, electron, plasma beams or arc to melt the feed the wire or powder material and add it to the build platform [33]. Robotic arms that hold the nozzle are used to allow for higher deposition rates, but with lower resolution [34].

### 2.3.2 Industrial applications of metal Additive Manufacturing

The main advantages of the application of metal Additive Manufacturing are: fabrication of complex geometries, reduction of waste material, and short design-to-product time frames; allows for improved efficiency in the manufacturing industrial sector. For this reason, and even though metal AM is not yet a mature technology, the application has already started by some industrial actors [30]

#### Aerospace

As a pioneer not only in the application but also in the development of metal AM technologies. Nowadays this technology has permeated into the majority of the sectors, and it is being applied from the manufacturing of rocket fueled liquid engines and different turbo-machinery components, to propellant tanks and valves [35].

Aircraft engine manufacturer General Electric (GE) Aviation uses machines from companies Concept Laser and Arcam to print fuel nozzles on the new LEAP engine [35, 36]. The resultant product is 25% lighter and more durable when compared to the original product, manufactured using traditional methods. Moreover, this new nozzle helps the engine achieve 15% higher fuel efficiency than the previous engine (CFM56) [37]. Another example can be found in Airbus, with the use of printers from the company Acronic, this company is producing large-sized airframe components [35]; and with use of machinery from Concept Laser it is producing wing brackets for the A350 XWB jet (figure 5), and turbine door hinges made of lightweight titanium (Ti64) for the A380 [38]. However in the last years, DED is the technology that has received considerable attention from the aerospace sector. It has been applied for the fabrication of turbo-machinery impeller blades as well as for the reparation of damaged components like engine combustion chambers [35, 39, 40].



Figure 5: (a) Fuel nozzle produced by GE Aviation for LEAP engine. Image credit: GE Additive,(b) Wing bracket of A350 XWB printed with Concept Laser machine and designed by Airbus. Image credit: Airbus Operations

The aerospace industry has benefited from the implementation of metal AM technology. With reduction of lead times by 70%, cut of non-recurring cost by 45% and components with mass reduction of 35% or higher [41].

## **2.4 AM produced Thermal Management Solutions for Electric Machines**

As mentioned in section 2.1, the management of thermal energy generated by the windings and core inside electric machines is critical to guarantee the reliability and efficiency at higher power densities, since higher temperatures are detrimental to these parameters. Therefore, better and more effective thermal management solutions must be devised.

In actuality, even though some research has been dedicated to the viability of applying AM solutions in the cooling of electrical machines, especially, electric motors. Very few examples can be found of the application of AM designs that make full use of the advantages provided by especially, metal additive manufacturing [42].

In section 2.1 a distinction between the two main qualifications of thermal management for electric motors was made: air and liquid cooling. With air cooling solutions being either active or passive, active solutions being a more complex and effective than passive ones, since it requires a method to create a flow of air for improved thermal evacuation.

### **2.4.1 Air cooling**

Passive air cooling, where natural convection takes place, is the simplest technique used for machine cooling. Since the flow cannot be controlled, the only way to enhance performance is by increasing the surface available for cooling. However, indiscriminate increase of this parameter can result in reduced performance. Therefore Topology optimization (TO), explained in section 2.5, is implemented to create a solution that maximizes both surface and airflow to produce an optimized cooling effect. The implementation of TO to solve thermal problems traditionally resulted in too complex geometries, to avoid this, additional constraints needed to be applied to realize attainable geometries. With the appearance of AM, and the ability to manufacture extremely complex geometries, this barrier is greatly reduced [43, 44, 45].

Heatsinks for passive cooling using TO have been compared with lattice structures and pin fin designs [46]. All manufactured in the same aluminum alloy and with the same dimensional limitations. The TO solution came on top when it came to heat evacuation, even with a smaller surface. An advantage explained by the increased airflow generated by natural convection of the topology optimized design. Demonstrating that a higher available surface doesn't translate to better performance.

Other applications of AM for the realization of passive air cooling heatsinks come with the printing of bio-inspired designed heatsinks. Brain corals inspired a design for a heatsink. The resulting structure, produced manufactured in AlSi10Mg using a SLM printer, maximized natural convection while maintaining a high surface area and even



Figure 6: Topology optimized shape manufactured for comparison against other geometries [46]

though a decrease in surface heat flux was detected. Therefore demonstrating these complex designs, realized with AM technologies, as superior heatsinks [47].

Forced convection or active air cooling electrical is used for machines with higher power densities, which makes use of fans to induce more air. Although, the maximization of surface area is still relevant, the objective becomes to minimize pressure drop over the fin structure instead of aiding natural convection. This is because a higher pressure drop reduces the airflow energy over the fins, in turn reducing cooling capacity. The use of lattice structures is a popular way to increase the surface of AM produces heatsinks. This lattice structures are a type of space-filling unit cell structures that can be tessellated along an axis without gaps between cells [48]. With the advent of additive manufacturing, that capability to create arbitrary structure from different materials has appeared. Allowing for research on the thermal capabilities of AM produced lattice structures [49, 50].

Another advantage of AM designs demonstrated in another study [51], is the capacity to achieve fin geometries that also provide structural support with a reduced mass. The solution chosen in the study opts to integrate the heat exchanger in the outer rotor motor design by making it the core of the motor, as clearly seen in figure 7. This allows the HE to be in direct contact with the stator teeth where the winding are located. The short distance minimizes thermal resistance resistance and the heat evacuation performance o the HE increases. Moreover, taking advantage of AM capabilities, the fins are designed with a curve that maximizes surface and consequently cooling performance while keeping weight low.

The ease of including shape patterns on fin surfaces thanks to AM to increase cooling performance of heat exchangers is also explored in another study from 2015 [52].

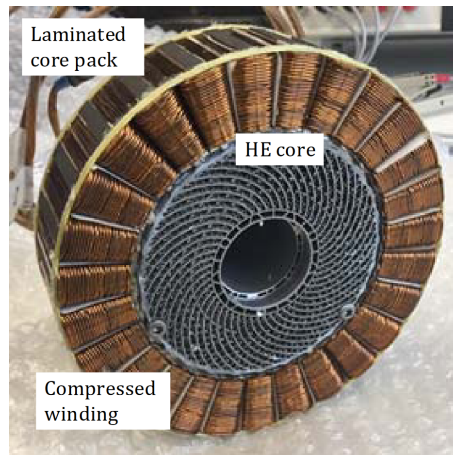


Figure 7: Heat exchanger as the motor core in the solar powered aircraft of study [51]

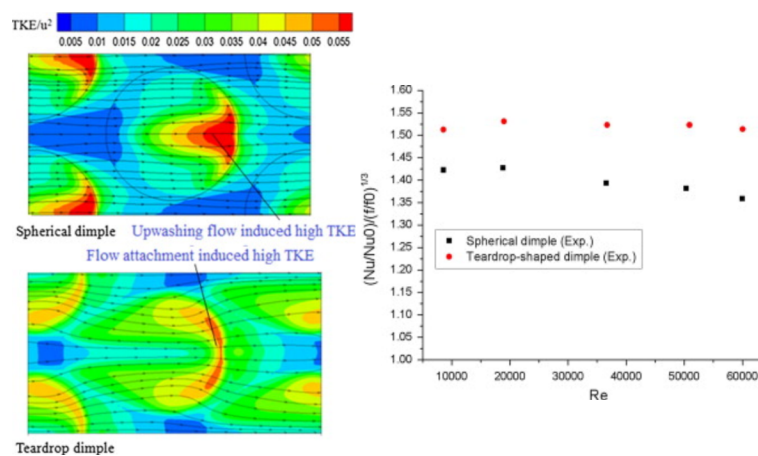


Figure 8: Left: Distribution of spherical and teardrop-shaped dimples on the fin surface. Right: Comparison of thermal performance of the two dimple designs using an overall thermal performance parameter in the Y axis and the Reynolds number of the flow in the X axis [52]

In this case, the fin designs included dimpled surfaces (spheres and teardrops). The researchers calculated that a fin surface with teardrop-shaped dimples showed up to 2 times better heat transfer performance compared to typically flat-surfaced fins.

## 2.4.2 Liquid Cooling

When air cooling, either passive or active, doesn't provide sufficient cooling performance. Liquid cooling appears as a more efficient but at the same time more complex cooling solution. The most common way to integrate water cooling has been through the use of water jackets that extract the heat from the outer stator, as mentioned in section 2.2.1, with the gap between stator and jacket presenting a thermal resistance that decreases the performance this set-up.

An alternative solution, difficult to implement until now, has been to integrate the cooling channels on the stator design and therefore bypass the gap problem. Now, with the advent of metal AM, this solution can be easily implemented, which unlocks

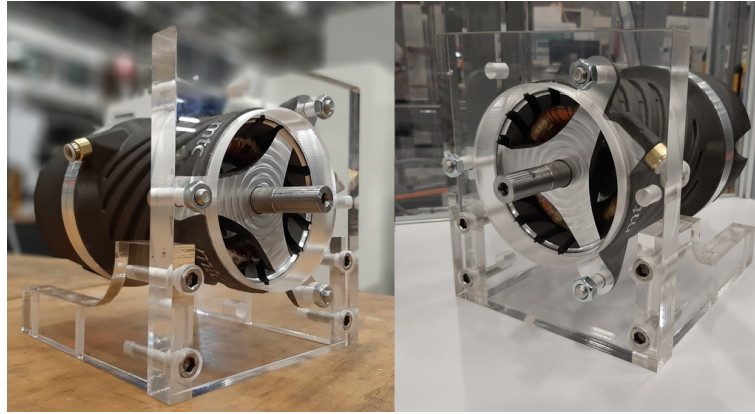


Figure 9: Two side views of the water jacket developed by the NCAM where ribs indicating the presence of cooling channels can be observed [53]

new levels of cooling performance. Additive manufacturing also allows for more customization, which in this case can be leveraged by easily producing geometry designs tailored for each individual motor's thermal requirement. This has been the focus of different studies.

In one study, the UK National Centre for Additive Manufacturing (NCAM) set to enhance the power density of electric by bypassing current manufacturing processes constraints with the application of AM techniques, with the focus of producing a liquid cooling solution. The outcome of the study is as follows: a roadmap was developed to progress with the implementation of AM in electric motor. However the more relevant outcome for this thesis, was the production of a prototype water jacket with embedded cooling channels that allowed the motor to function on a higher power setting without overheating, cut weight by 10% and reduced the size by 30% compared to the water jacket used previously [53]. While in another study [54], the European Powder Metallurgy Association (EPMA) manufactured an aluminium cooling jacket (figure 10a) provided enough cooling to increase the power in the motor and achieve an increase in performance of 37% when compared to motor with the previous cooling system.

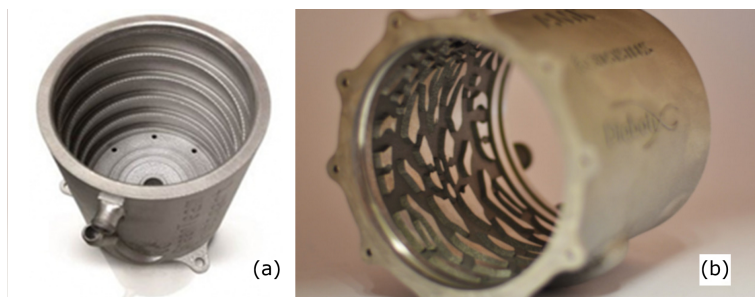


Figure 10: (a): Cooling jacket developed by EPMA [54]; (b): Diabatix solution for optimized electric motor cooling jacket [55]

Another interesting application of AM technology to fabricate a cooling jacket also makes use of Topology optimization to achieve a greater cooling performance of the jacket. The company Diabatix in conjunction with Team Delft University of technology race car, this new jacket achieved a temperature reduction of 21% in the motor that re-

duced battery drain by 80%. The design, which was assisted by AI, parted from the traditional spiral channels and achieved an organic looking pattern as shown in (figure 10b). One last example of this type of solution was used by an racing team from a Chinese university on a 1,2 kW electric motor inserted in the wheel hub [56], however, this solutions opts to used a traditional design without fully exploiting AM capabilities.

## **2.5 Topology Optimization for heat exchangers**

Topology optimization is a design methodology that identifies the optimal placement and distribution of materials within a specified design domain. This approach significantly enhances design flexibility, surpassing the capabilities of traditional size and shape optimization. While size optimization focuses on modifying variables like the thickness or cross-sectional areas of structural components, and shape optimization alters the geometric characteristics of pre-established structural layouts, topology optimization involves determining the optimal configuration and location of voids and solid regions in a material, effectively dictating the most efficient material layout [57]. This method offers a substantial increase in the potential for innovative design solutions by enabling the design of complex structures specific to certain performance criteria.

The TO workflow for heat excahngers includes four stages: Design parametrization, heat transfer modeling, optimization process and final realization. And compared to mechanical structure TO, issues can appear en each stage when working in TO for thermodynamic applications, issues can appear in any step, either related to fluid flow or heat transfer characteristics [58]. The complex final structures of Heat exchangers pose significant challenges for practical applications of TO. While maximizing heat transfer is a primary goal, pressure loss must also be considered, often using a weighted-sum objective function or multi-objective optimizers [59]. Although advances in additive manufacturing (AM) have enhanced the realization of optimized designs, post-treatments of the printed products is necessary to achieve satisfactory product [60]. However, not many studies or reviews exist addressing TO application in microfluid devices, heat transfer systems, and fluid-based problems are sparse, with few considering manufacturing constraints directly in heat exchangers TO [61, 62].

### **2.5.1 Design parametrization**

Design parametrization is the selection of optimization variables that define design configurations, linking design variables to physical properties via interpolation functions. This choice heavily influences the output results of the TO [63], and the type of parametrization varies based on the TO method, problem specifics, and physical

phenomena.

### Density-based method (DBM)

It uses densities to define fluid and solid phases, where density  $\gamma$  equals 0 for solid and 1 for fluid, employing inverse permeability to model fluid flow. Characterized by the SIMP approach, this method uses penalization to minimize intermediate densities [64].

### Level-set method (LSM)

The level-set method defines phase interfaces using a level-set function, enhancing boundary response accuracy. In this method, the function  $\phi$  indicates material phases if positive, interfaces at zero, and voids if negative. This method, utilized in TO for heat exchangers, offers a precise interface representation crucial for scenarios where interface properties impact performance [65]. LSM typically avoids re-meshing, benefiting HEs where heat transfer relies on near-interface flow dynamics. However, initial setup heavily influences outcomes, and LSM generally converges slower than density-based methods, often requiring regularization techniques to stabilize the solution [66].

### Direct explicit method

Direct explicit parametrization, uses functions or arrays to clearly define interfaces, it is applied for shape optimization [67], but not as common in TO for heat exchangers, where it is used despite its ability to avoid numerical issues seen with implicit methods [68].

Table 1: Comparison of parametrization methods.

Parametrization	Advantages	Disadvantages
Density-based	Fixed mesh Proved for TO	No interface described Numerical instabilities Modified governing equations
Level-set	Crisp description of interface profile No re-meshing	Slow convergence Dependant of initial configuration Numerical artifacts
Direct explicit	Interface described explicitly Stright-forward and simple	Only for simple geometries

## 2.5.2 Heat Transfer Modelling

Heat transfer modelling is described by four primary equations: continuity, momentum, and energy balance for fluids and solids. These equations account for variables such as specific heat, thermal conductivity, velocity, temperature, pressure, fluid dynamic viscosity, and density, incorporating time and a heat source term. Additionally,

a fictitious force, derived from inverse permeability is applied in density-based TO to simulate the solid phase's impact on the fluid. Solving these equations at each iteration is critical for determining the objective function values. Being common practice to simplify assuming steady-state conditions and incompressible flows.

### **Finite element method (FEM)**

The FEM was initially proposed by Hrennikoff and McHenry to solve structural problems and has evolved into a technique for solving partial differential equations by discretizing domains into finite elements. FEM is highly flexible and provides accurate results across various physics applications [69].

In TO of heat exchangers, FEM has been widely employed to handle steady-state laminar flows in 2D and 3D contexts. For example, Dede [70] has utilized FEM in optimizing liquid-cooled heat sinks and HE channels, respectively. Additionally, some studies have addressed turbulent flow in topology optimized heat exchangers using FEM to solve Reynolds averaged Navier-Stokes equations, like Zhao et al. [71] who employed it for cooling channels.

### **Finite volume method (FVM)**

The Finite Volume Method involves dividing the design domain into control volumes, integrating governing equations over each control volume, and applying the divergence theorem to summarize boundaries over each one [72]. Reliable in CFD, this method was initially applied in topology optimization TO for heat conduction by Gersborg-Hansen et al. [145] and later for steady-state laminar flow in heat exchangers [73].

FVM's conservativeness across each CV makes it suitable for CFD challenges [72]. However, despite its advantages, the use of FVM remains limited, mainly due to the lack of FVM-based TO software and mesh dependency of the results. This can complicate the design of accurate schemes without appropriate filters [74].

### **Extended finite element method (XFEM)**

This method enhances the Finite Element Method by adding an extra degree of freedom at nodes near discontinuities [75, 76]. XFEM has been integrated with the LSM for topology optimization in 2D and 3D heat transfer problems [77, 78]. XFEM and LSM together capture interfaces effectively during TO while also significantly increase the computational load. Despite its detailed interface description, XFEM is rarely used in heat exchanger TO due to its computational intensity and stability issues, similar to FEM, caused by non-conservative fluxes [79]. Moreover, transient problems require small time steps with XFEM to accurately depict rapid physical property changes, like temperature variations at interfaces [80].

### **Lattice Boltzmann method (LBM)**

The Lattice Boltzmann Method (LBM) is used for solving transport equations, representing macroscopic equations through a set of Boltzmann transport equations within a lattice gas framework [81].

Table 2: Comparison of Solvers

Solver	Advantages	Disadvantages
FEM	High availability in TO Physics flexibility	Not ensuring the conservation law locally Numerical instabilities for convection
FVM	Locally ensuring conservation law Suitable for CFD problems	Low availability in TO Accuracy in high order scheme designs High mesh quality
XFEM	Efficient in big data problems	Expensive and complex computation Scalability with number of objective functions
LBM	Efficient in big data problems	Expensive and complex computation Scalability with number of objective functions

### 2.5.3 Optimization

When applying TO on heat exchangers, after utilizing heat transfer solvers to compute objective functions, an optimization process adjusts the design variables to optimize these functions under established constraints. Thermal performance objectives include: minimizing average temperature rise, thermal compliance, and thermal resistance, or maximizing heat exchange and recoverable thermal power [82, 83, 84]. Hydraulic performance is also often a constraint or objective, typically focusing on minimizing pressure drop and flow energy loss.

#### Gradient-based optimization

The gradient-based method computes the gradients of the objective functions relative to design variables, using the efficient adjoint method to calculate the gradients [85]. In topology optimization of heat exchangers, different gradient-based optimizers like: MMA, GCMMA, SLP, SQP, Steepest descent, Tosca, Reaction-diffusion, Hamilton-Jacobi, and the Null Space algorithm are employed [86, 87].

#### Genetic algorithm (GA)

Inspired by the biological processes of chromosomes and genes. It starts with a random generation of an initial solution that maximizes diversity. Afterwards, the fitness values for each chromosome are assessed using objective functions. It is particularly effective for multi-objective problems, managing multiple candidates simultaneously to develop the Pareto front [88].

## Bayesian optimization (BO)

BO consists of two primary components: statistical modeling and the acquisition function. The first step consists in generating a random set from which a mean vector and covariance matrix are derived using Gaussian process regression. After this, an acquisition function is then optimized to guide the next objective function optimization [89].

Table 3: Comparison of Optimizers

Optimizer	Advantages	Disadvantages
Gradient-based	Efficient for the large-design-variable-number problems High availability in TO	Deficiency in multi-objective problems Local optima
Genetic algorithm (GA)	Gradient-free Global Optima Efficient in multi-domain problems	Slow convergence Randomness
Bayesian Optimization (BO)	Efficient in big data problems	Expensive and complex computation Scalability with number of objective functions

## 2.6 Topology Optimization in COMSOL

The topology optimization for this thesis has been carried out using the solver and multiphysics software, COMSOL Multiphysics. This software can be applied to electrical, mechanical and fluid dynamics applications as well as providing an Integrated Development Environment. Inside the optimization module, two classes of problems can be found: the design problem and the inverse problem; being the focus of the thesis the design problem. This aims to find the control variables that lead to the best performance of the model with an objective function.

The optimization module facilitates considering any model input as a control variable and any output as the objective function. With the purpose of the optimization being to locate the control variables which minimize or maximize the objective function value under the set constraints.

### 2.6.1 Optimization algorithms

Taking into account two control variables input parameters and taking into account the constraints within the problem, a feasible design space is defined with specific upper and lower limits, as well as areas of infeasibility of the design. The optimal

solution is identified at the peak of the control plot, representing the maximum value of the objective function as represented in figure 11.

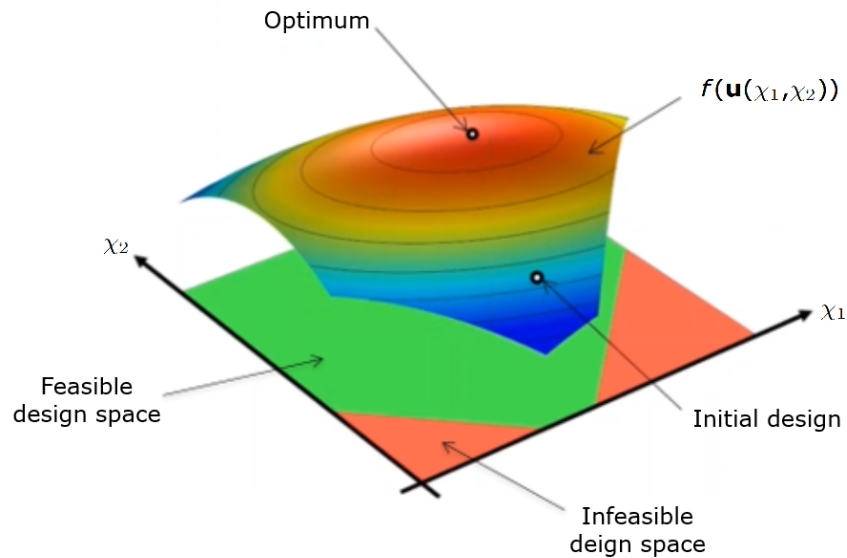


Figure 11: Design domain defined by two variables  $(x_1, x_2)$  where infeasible design space represents the limits established by the constraints (red) and the optimum solution is presented in the top of the curve while the initial design starts at lower in the curve, representing a non optimal solution

The gradient-based optimization technique utilizes the derivative of the cost function relative to the design variable to conduct the sensitivity analysis. The zero gradient point indicates either a maximum or minimum, while the second derivative determines whether this point is a maximum or minimum. If the cost function can't be differentiated or the gradient is unstable, the option to use the Gradient-Free method is allowed, where optimization is achieved using a triangulation algorithm, which computes solutions at three points and then moves towards the area of maximum or minimum value. A recurring challenge emerges when multiple minima or maxima within the design space occur. Leading the algorithm to converge on a local minimum or maximum instead of a global optimum. This case is heavily influenced by the initial starting point.

Three gradient based solvers are available. Sparse Nonlinear Optimizer algorithm (SNOP) , employs sequential quadratic programming algorithm with limited-memory quasi-Newton approximations to the Hessian of the Lagrangian. Being mainly used for nonlinear problems and applied to any cost function without limitation on the constraints. Method of Moving Asymptotes (MMA) is suitable for managing problems with many control variables. And Lavenber-Maraquardt, a fast converging method that however doesn't support constraints and needs least-squares type objective functions.

## 2.6.2 Optimization Theory

The optimization problem can be defined in the following way:

$$\begin{cases} \min_{\xi} Q(\xi) \\ \xi \in C \end{cases} \quad (2.2)$$

Where the control variables are represented by  $\xi$  and  $Q$  is the scalar-valued objective function. with  $C$  being the feasible set, which with sufficient continuity, can be presented as a set of inequality constraints,  $G$  represents a vector valued function:

$$C = \{\xi : lb \leq G(\xi) \leq ub\} \quad (2.3)$$

When addressing multiphysics through a Partial Differential Equation (PDE), it is preferable to parameterize the problem making use of the control variable and refine the cost function contingent on the solution to the PDE. Consequently, the objective function is dependent on the solution of the PDE, and therefore, on the control variables. The discretization of the system is applied through a series of equations:  $L(u(\xi), \xi) = 0$ , where  $u$  represents the solution to the PDE, and  $\xi$  denotes the control variable. This PDE is subsequently integrated as an equality constraint within the overarching optimization problem, establishing a comprehensive PDE-constrained optimization framework.

$$\begin{cases} \min_{\xi} Q(\xi) \\ L(u(\xi), \xi) = 0 \\ \xi : lb \leq G(\xi) \leq ub \end{cases} \quad (2.4)$$

In the case of the software optimization module, the objective function can be defined as the sum of the contributions:

$$Q(u, \xi) = Q_{global}(u, \xi) + Q_{probe}(u, \xi) + \sum_{k=0}^n Q_{int.k}(u, \xi) \quad (2.5)$$

Where  $n$  represents the domain of the problem.  $Q_{global}$  is the global contribution of the objective function  $Q$ ;  $Q_{probe}$  in the objective function  $Q$  in a confined point of the geometrical entity; and  $Q_{int,k}$  represents the integral of the objective function in a set of restricted number of geometric entities in the same dimension. The sum impact of each component in the objective function is as the cumulative sum of individual contributions from the same optimization interface. This framework facilitates the application of a weighting coefficient to each contribution, hence allowing the customization of optimization by scaling the various contributors of the objective function.

Regarding the constraints, the interface of the optimization differentiates the bounds in those applied on the control variables to those defined with pointwise or integral inequalities and global inequality constraints.

### 2.6.3 Topology Optimization

Density model may be the oldest and most employed method use to date. It consists on the discretization of the design domain, using a control variable which is associated to fictitious material on nodes. By interpolating the control variable from 0 to 1, the physical governing equation is can be solved when the variable equals 1. Conversely, when the control variable is set to 0, an equation for the fictitious material is solved.

Furthermore, it is common to apply a filter that induces a minimum length scale on the design variable as a constraint to avoid the ill-posedness problem. In finite element analysis, the design control variable ( $\gamma$ ), and the optimal structure layout is derived via topology optimization, which determines for each element in the design domain whether it contains a material ( $\gamma = 1$ ) or is assigned to another category ( $\gamma = 0$ ). The problem can there be formulated as:

$$\left\{ \begin{array}{l} \min_{\gamma} : F = F(u(\gamma), \gamma) = \int_{\Omega} f(u(\gamma), \gamma) dV \\ \text{subjected to :} \\ G_0(\gamma) = \int_{\Omega} \gamma(x) dV - V_0 \leq 0 \\ G_i(u(\gamma), \gamma) \leq 0, i = 1, \dots, M \end{array} \right. \quad (2.6)$$

Where the problem intends to find the material distribution that minimizes the objective function ( $F$ ) which is subjected to the constraints:  $G_0$ , that ensure the material volume generated is smaller that the domain value; and  $G_i$ . And where  $u$  represents the state variable field that satisfies the state equation.  $\gamma$  is the control variable of the optimization problem and defines the material distribution,  $\Omega$  represents the design domain within which,  $\gamma = 0$  represents liquid material and  $\gamma = 1$  solid. Lastly, the domain discretization in  $N$  finite elements, and result in that for each discretization a value of  $\gamma$  equal 0 or 1 is given. This results in the following:

$$\left\{ \begin{array}{l} \min_{\gamma} : F = F(u(\gamma), \gamma) = \int_{\Omega} f(u(\gamma), \gamma) dV \\ \text{Subjected to :} \\ G_0(\gamma) = \int_{\Omega} \gamma(x) dV - V_0 \leq 0 \\ G_i(u(\gamma), \gamma) \leq 0, i = 1, \dots, M \\ \gamma_i = 0 \text{ or } 1, i = 1, \dots, N \end{array} \right. \quad (2.7)$$

The control variable only has discrete values 0 or 1. However, the large number of variables in TO makes solving the problem difficult, therefore applying continuous values. Since the continuous values can't be associated to either solid or liquid, a penalty method is applied to the optimization problem. The penalised material volume ( $\gamma_p$ ) is used of material interpolation with the use of a penalization to achieve 0-1. The three interpolation schemes that can be found in the COMSOL Optimization module include are SIMP (Solid Isotropic Material with Penalization), RAMP (Rational Approximation of Material Properties) and Darcy. Where  $\gamma_p$ ,  $p$  being the penalization parameter, is

represented for each one as:

$$\text{SIMP: } \gamma_p = \gamma_{min} + (1 - \gamma_{min})\gamma^{p_{simp}} \quad (2.8)$$

$$\text{RAMP: } \gamma_p = \gamma_{min} + \frac{\gamma(1 - \gamma_{min})}{1 + q(1 - \gamma)} \quad (2.9)$$

$$\text{Darcy: } \gamma_p = \frac{q(1 - \gamma)}{q + \gamma} \quad (2.10)$$

The SIMP and RAMP interpolation schemes are reliable when working with solid mechanics, while the Darcy scheme is more adequate for fluid mechanics problems. Through the use of a continuous design variable, it is possible to apply gradient-based algorithms, which allows the evaluation of the derivative of the objective function with respect to the control variable. This is critical for optimizing the function, enhancing the precision and efficiency of the solution process. finally, the continuous problem is presented as follows:

$$\left\{ \begin{array}{l} \gamma^{min} : F = F(u(\gamma), \gamma) = \sum_i \int_{\Omega_i} f(u(\gamma_i), \gamma_i) dV \\ \text{subjected to :} \\ G_0(\gamma) = \sum_i u_i \cdot \gamma_i dV - V_0 \leq 0 \\ G_i(u(\gamma), \gamma) \leq 0, j = 1, \dots, M \\ \gamma_{min} \leq \gamma_i \leq 1, i = 1, \dots, N \end{array} \right. \quad (2.11)$$

For 3D simulation, a density filter works to avoid ill-posedness of the optimization problem. Moreover, a density filter requires a minimum length-scale,  $R_{min}$ , on  $\gamma$ . The filter, known as Helmholtz-type PDE filter can be expressed as:

$$\gamma_f = R_{min}^2 \nabla^2 \gamma_f + \gamma_c \quad (2.12)$$

Where  $\gamma_f$  is the filtered material volume factor. The continuous filtered variable is discretized using linear polynomials, this simplifies the optimization process, a the cost of the filtered design variable exhibiting a band with intermediate densities. The presence of intermediate control variables can induce a non-optimal final design. To minimize this problemn, the intermediate band is diminished by projecting the filtered design variable field towards the extremes (0 and 1). The projection used is based on the hyperbolic tangent function, which narrows the range of intermediate densities and enhances the physical relevance of the design outcome:

$$\gamma = \frac{\tanh(\beta(\gamma_f - \gamma_\beta)) + \tanh(\beta\gamma_\beta)}{\tanh(\beta(\gamma_\beta)) + \tanh(\beta\gamma_\beta)} \quad (2.13)$$

### 3. TOPOLOGY OPTIMIZED DESIGN

#### 3.1 Optimization of the desired geometry

The purpose of this work is to cool of an inner rotor electric motor, whose outer dimensions are: diameter 80 mm and width 50 mm. Specifically through the use of water cooling and taking advantage of topology optimization in thermal applications.

The most common way to solve this problem would include defining a 3D geometry in the shape of a cylinder with the aforementioned width of 50 mm and inner diameter of 80 mm. However, 3D simulation and computation possesses the disadvantage of being very computationally intensive and therefore, early on in the concept definition phase of the problem, it was considered that the simulation may be carried in a 2D environment. To geometrically achieve this, cylinder with difference between outer and inner diameters that tends to 0 is considered. And then, the curved surface of the cylinder is unfolded, conforming a rectangle. For the sake of simplification and without sacrificing the practical application of the design, the rectangle width is set to 50 mm and the length to 252 mm, a rounding up in millimeters of the circumference of circle of 80 mm:  $\pi \times 80 = 251,32$ .

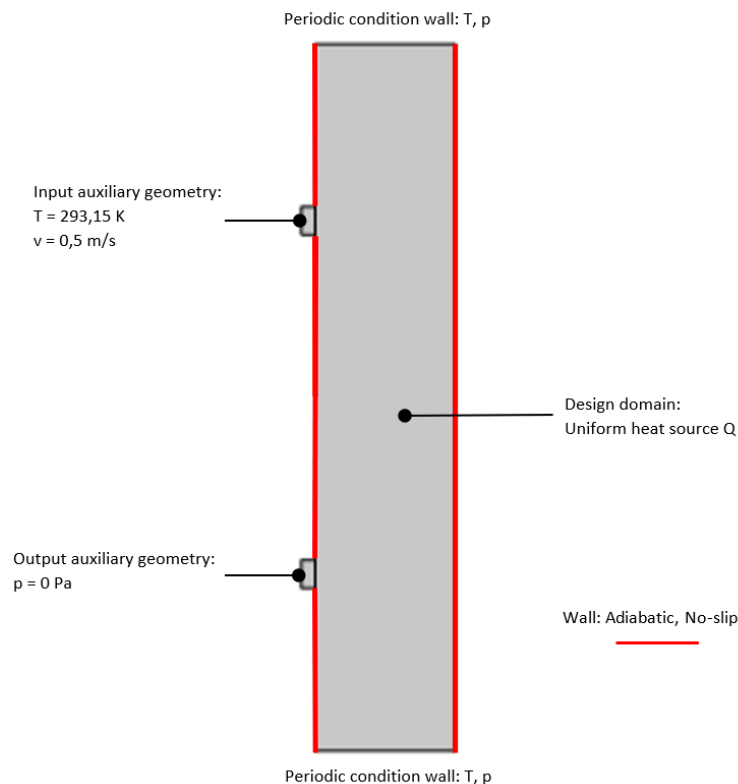


Figure 12: Design domain (50 x 252 mm) with auxiliary geometries (5 x 10 mm)

A problem that arises from this approach is the disconnect between the opposing 50mm edges. This two edges, result of the unfolding of the curved face, are part of

the continuous surface that has been split. To overcome this feature, a continuous condition for flow of liquid and temperature is established, known in COMSOL as Periodic condition. Before proceeding with the study, the functionality and reliability of the periodic condition has been checked to certify the feature works in both directions even though in COMSOL one edge is recognized as the source and the other as the destination. The rest of

With the design domain defined, simulations using flow, temperature and a combination are set up and undertaken. Established 15 years ago by E.M. Dede[70]: two single physics problems, one of heat conduction and a second for laminar flow are conducted, to later combine the problems in a Multi-physics problem. For the problems the following parameters are set: a uniform heat source of 100 Watts is applied to the surface of the design domain, and through the input of the top auxiliary geometry a water flow at a temperature of 293,15 K and velocity of 0,5 m/s is introduced and exits through another auxiliary geometry which functions as output. The auxiliary geometries are absent of optimization and are present to make the model function properly. Lastly, for simplicity sake the edges are assumed to be adiabatic and with no slip, meaning velocity of flow in surface is 0 m/s. The walls also assume an adiabatic condition.

### 3.1.1 Heat Conduction Problem

This single physics problem is aimed at solving an objective equation whose objective is to extract the maximum amount of heat from the design domain. Within the domain, each element is associated with variable  $\gamma$ , which is related to the thermal conductivity through the interpolation scheme. Therefore the range of values from 0 to 1 represents on the lower end, the less conductive material, and in the higher end the more conductive material.

#### Governing equation

The governing equation for this problem for this problems is Fourier's law:

$$Q = -\nabla(k(\gamma)\nabla T) \quad (3.1)$$

Where T is the temperature state variable, Q the volumetric heat generation in the domain and  $k(\gamma)$  the thermal conductivity depending on the design variable. For this problem, the Q value is set to  $10 \frac{W}{m^3}$ .

#### Objective function

The theoretical objective function for the heat conduction single physics problem is the dissipation of heat transport capacity:

$$J = \int_{\Omega} (k\nabla T^2) d\Omega \quad (3.2)$$

However, Dede[70] defines this objective function as the equivalent to minimizing the main temperature in the design domain,  $\Omega$ , when under a constant heat generation. Which is the actual objective function applied.

### Interpolation scheme

For the thermal conduction problem the chosen interpolation scheme is SIMP, defined in equation (2.8). Where  $\gamma$  is the aforementioned control variable,  $\gamma_p$  is the penalized variable,  $p_{simp}$  is the penalization coefficient and has a value of 3, and  $\gamma_{min}$  is valued at 0,001. For the of simplifying the simulation, the thermal conductivity values of the most conductive material  $k_{max}$  is set to  $1 \frac{W}{mK}$ . And since with the interpolation scheme, thermal conductivity is calculated the following way:

$$k_\gamma = k_{max}\gamma_p \quad (3.3)$$

The thermal conductivity values for aluminum the most conductive material  $k_{al}$  and water the less conductive  $k_w$  are calculated the following way:

$$\gamma = \begin{cases} 1 : k_{al} = k_{max} = 1 \frac{W}{mK} \\ 0 : k_w = k_{min} = 0.001 \frac{W}{mK} \end{cases} \quad (3.4)$$

With all the previous statements, the mathematical expression of the heat conduction problem is as follows:

$$\left\{ \begin{array}{l} \text{Find : } \gamma \\ \text{Minimizing : } J = \int_{\Omega} (k_\gamma \nabla T^2) d\Omega \\ \text{Subjected to :} \\ \int \gamma d\Omega_d - V_{max} \leq 0 \\ Q = -\nabla(k(\gamma)\nabla T) \\ 0 \leq \gamma \leq 1 \\ \text{Given : } k_\gamma = (0,001 + 0,999\gamma^{p_{simp}})k_{max} \end{array} \right. \quad (3.5)$$

Where the subjections represent: in the first place the ratio of material in respect to the total domain area must be always have a lower absolute value; and secondly, the range of values gamma can take in the different iterations. Moreover, for the proposed problem, a triangular mesh automatically generated with a manual maximum element size set to 1 mm. And the optimizations solver employed is MMA with SIMP as the interpolation scheme, as observed in equation (3.5).

### Results

Three different studies have been carried out for the eat conduction problem. All with the same objective functions, but with different ratios of total material surface, or volumetric fraction, present in each one of the three tests carried out. Volumetric

fraction can be expressed as follows:

$$V_{target} = \frac{\int \gamma d\Omega_d}{V_{max}} \quad (3.6)$$

■  $V_{target} = 0,5$

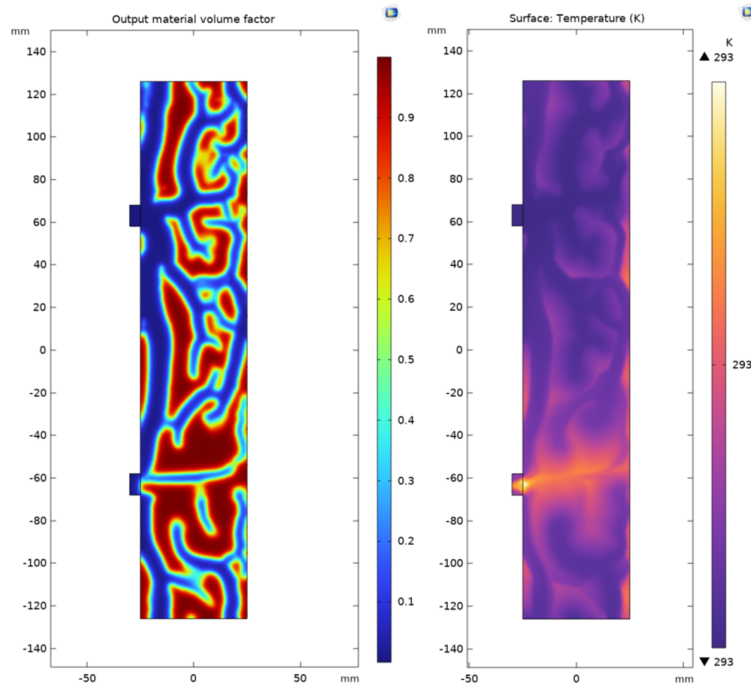


Figure 13: For  $V_{target} = 0,5$ . (a): Material distribution inside the domain. (b): Temperature map for material distribution in (a)

In the figure on top, and in the figure at the bottom a clear correlation can be observed between the temperature and flow speeds with the resulting material distribution.

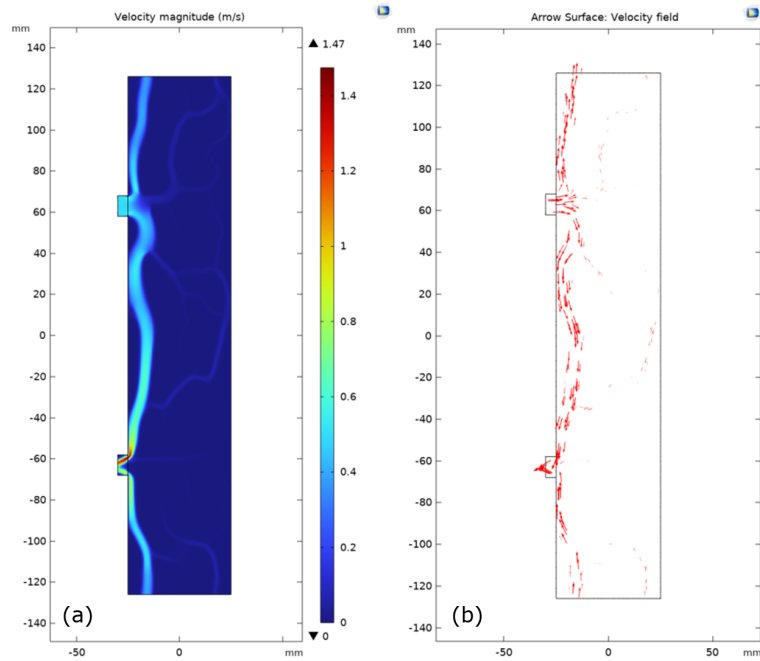


Figure 14: For  $V_{target} = 0,5$ . (a): Velocity of the fluid inside the domain. (b): Vectors of direction for flow indifferent parts of the design domain. With the data offered in both figures, the path and velocity of the liquid inside the domain can be distinguished

■  $V_{target} = 0,4$

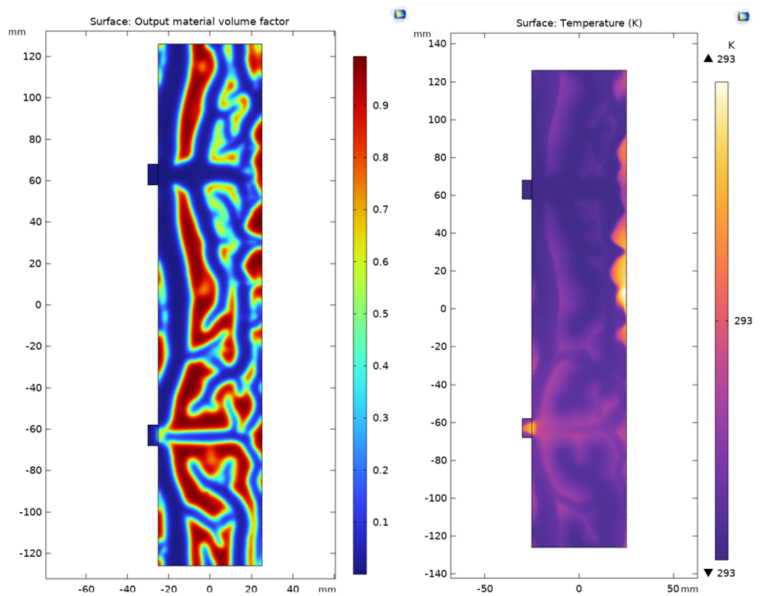


Figure 15: For  $V_{target} = 0,4$ . (a): Material distribution inside the domain. (b): Temperature map for material distribution in (a)

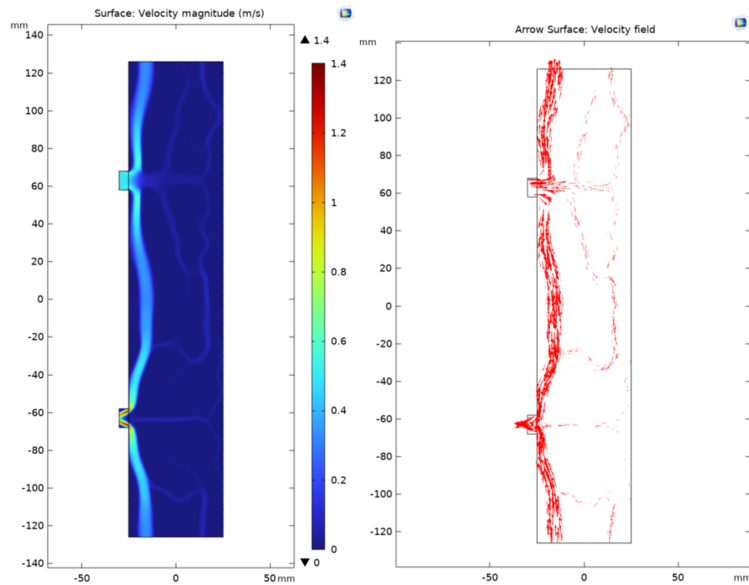


Figure 16: For  $V_{target} = 0,4$ . (a): Velocity of the fluid inside the domain. (b): Vectors of direction for flow indifferent parts of the design domain. With the data offered in both figures, the path and velocity of the liquid inside the domain can be distinguished

■  $V_{target} = 0,3$

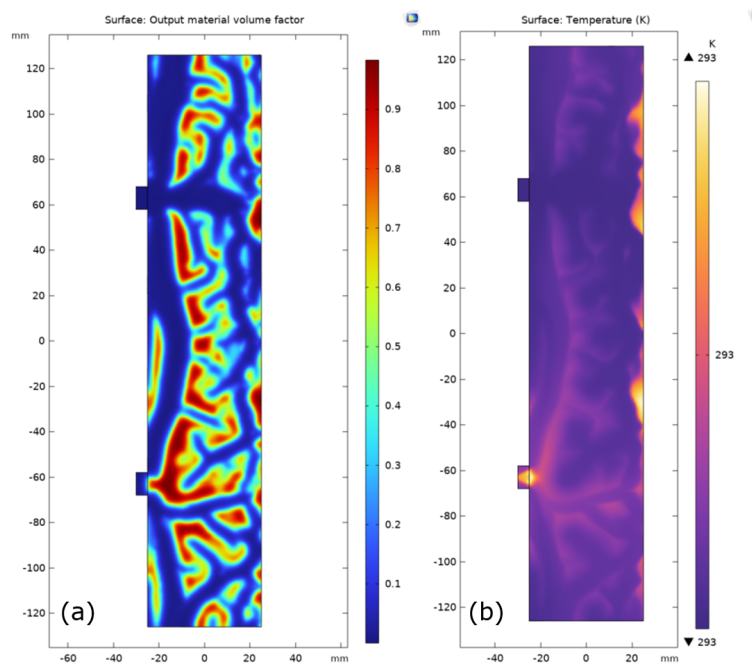


Figure 17: For  $V_{target} = 0,3$ . (a): Material distribution inside the domain. (b): Temperature map for material distribution in (a)

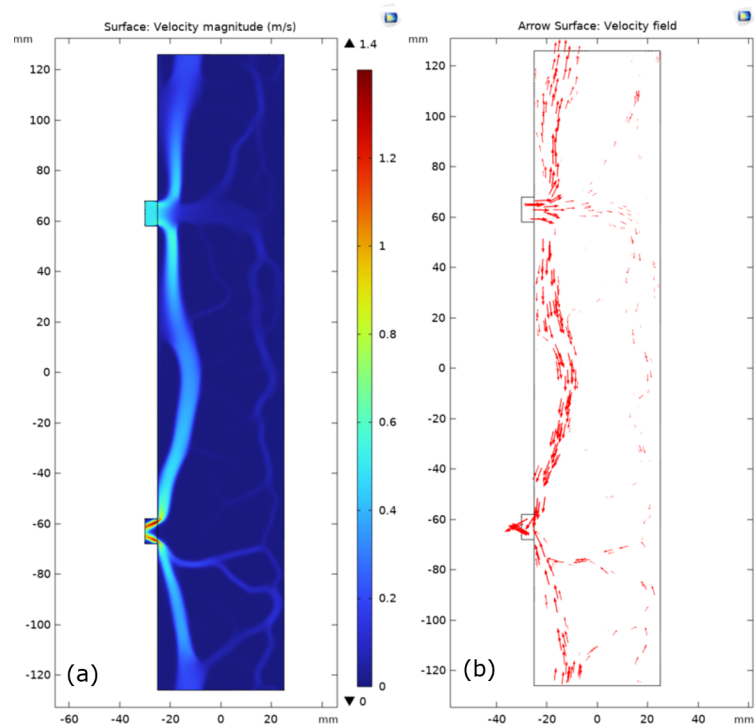


Figure 18: For  $V_{target} = 0,3$ . (a): Velocity of the fluid inside the domain. (b): Vectors of direction for flow indifferent parts of the design domain. With the data offered in both figures, the path and velocity of the liquid inside the domain can be distinguished

With the three results presented, it can be clearly observed that material presence is directly proportional to the volumetric factor for problem as observed in part (a) of figures 13, 15 and 17. What can also be concluded from these figures, is that the material distribution is focused in the same locations but with decreased material presence. For the conditions established, the hotspot temperature for the three problems is the same however, in the (b) section of the figures mentioned already, the location of these hotspots and the overall temperature map of the results change, with the overall material distribution being discernible by colors related to higher temperatures in contrast to the colors that represent the fluid channels that represent lower temperatures.

From figures 14, 16 and 18 it can also be recognized that the fluid channels are greatly affected by the volumetric factor, while the maximum flow speed is similar in all three solutions, thanks to a material presence similar in close proximity of the output channel and recognizable in section (a) of the figures. It can be also recognized that for a volumetric factor of 0,3 there is a larger presence of smaller channels that distribute flow through all the domain, and a lower flow speed in the main channel that runs parallel to the left vertical edge from input to output, when compared to the result for a volumetric factor of 0,4 and specially for 0,5. In the later case being specially pronounced and observable in figure 13(b).

### 3.1.2 Fluid Flow Problem

For this single physics problem the objective of the optimization is to minimize the flow power losses inside the domain. The Navier-Stokes equations are applied in order for the iteration process to achieve the optimal distribution of material inside the domain to achieve the minimal value of the objective function.

The design domain maintains the geometry presented in figure figure 12 and the flow input speed is also maintained at 0,5 m/s. The pressure at the output is set to 0 Pa as dictated in the COMSOL multi-physics Cyclopedia[90] for the application of Navier-Stokes equations.

#### Governing equations

A part from the Navier-Stokes equations, the continuity equation and the assumption of stationary laminar flow with incompressible fluid, will also govern the equations for this problem:

$$\begin{cases} \rho_{fl} \cdot (u \cdot \nabla)u = -\nabla p + \mu(\nabla^2 u) + F \\ \rho_{fl} \cdot (\nabla)u = 0 \end{cases} \quad (3.7)$$

Where  $F$  represents the Brinkman friction term that introduces a penalization for the fluid velocities in the solid material for the design domain. Represented by the volumetric force, this is only considered in the large rectangular geometry, the input and output rectangles being exempt.  $F$  is function of the control variable:

$$F = \alpha(\gamma) \cdot u \quad (3.8)$$

In this case,  $\alpha$  represents the inverse permeability of the porous medium and is defined as a function of the design variable  $\gamma$ .

#### Objective function

The purpose of this single physics problem is to reduce the fluid power losses to the minimum possible. When this this accomplished, the difference between the inlet and outlet pressure also minimizes. Therefore, to simplify the problem, this is the objective function applied:

$$J = p_{in} - p_{out} \quad (3.9)$$

#### Interpolation scheme

As a pure fluid dynamics problem, the interpolation selected is SIMP even though Darcy is more appropriate for fluid dynamics, because of the posterior integration of the two single physics problems. Applying the interpolation scheme to the inverse permeability, it is defined as follows:

$$\alpha = \alpha_{max} \gamma_p \quad (3.10)$$

The values of inverse permeability are for both fluid material (water) and solid material (aluminum) are defined as defined as  $k_{water} = 1 \cdot 10^7 \frac{1}{m^2}$  and  $k_{aluminum} = 1 \cdot 10^{11} \frac{1}{m^2}$ . Resulting in the following:

$$\gamma = \begin{cases} 1 : k_{al} = k_{max} = 1 \cdot 10^{11} \frac{W}{mK} \\ 0 : k_{al} = k_{max} = 1 \cdot 10^7 \frac{W}{mK} \end{cases} \quad (3.11)$$

Where  $p_{in}$  is inlet pressure and  $p_{out}$  is the outlet pressure. Finally, the expression of the optimization of the fluid flow problem is:

$$\left\{ \begin{array}{l} Find : \gamma \\ Minimizing : J = p_{in} - p_{out} \\ Subjectedto : \\ \int \gamma d\Omega_d - V_{max} \leq 0 \\ 0 \leq \gamma \leq 1 \\ Given : k_{\gamma} = (0,001 + 0,999\gamma^{p_{simp}})k_{max} \end{array} \right. \quad (3.12)$$

Where the subjections represent: in the first place the ratio of material in respect to the total domain area must be always have a lower absolute value; and secondly, the range of values gamma can take in the different iterations. Moreover, for the proposed problem, a triangular mesh automatically generated with a manual maximum element size set to 1 mm. And the optimizations solver employed is MMA with SIMP as the interpolation scheme, as observed in equation (3.5).

## Results

For the Fluid flow problem seen in figure 19, solid material characterized by the control variable value of 1, and liquid material represented by the control variable value 0; follow the distribution so that the pressure difference in the domain when comparing the input and output pressures is a minimal as possible. The flow of coolant, water, is divided in two in the input and a curved surfaces formed by aluminum re-direct it to the output. The flow of liquid can be further observed in figure 20a, where the direction vectors are represented and the division the flow can clearly be observed; and in figure 20b, where the velocity of the flow is represented.

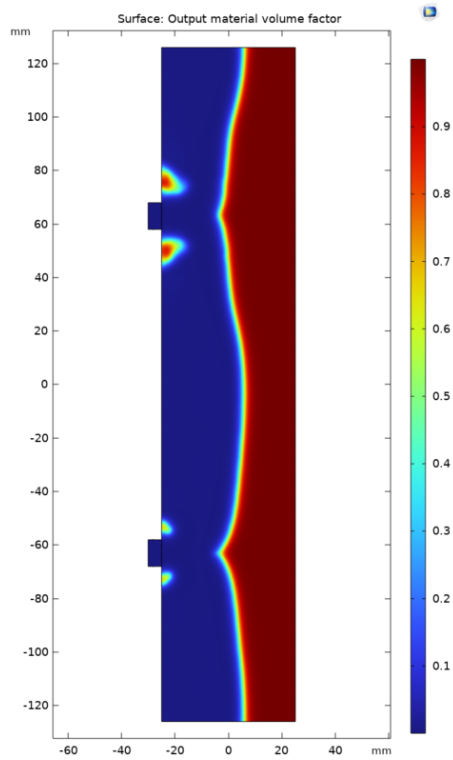


Figure 19: Topology optimization result of the Fluid flow problem

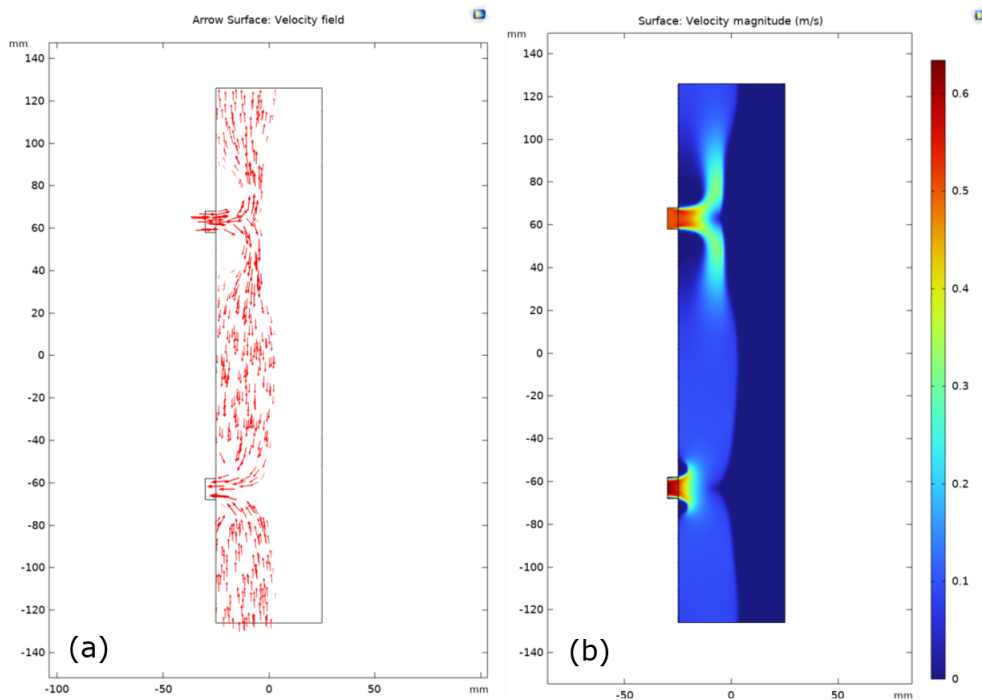


Figure 20: (a): Velocity field showing the regions of the geometry with circulating flow; (b): Color gradient plot of velocity magnitude showing the velocity value of the flow inside the domain

Finally, in figure 21 the pressure map of the domain, a difference of 404 Pascals can be observed inside the domain. With the higher pressure spot located in point of contact

between the input flow and the aluminum material, it correlates to the point present in figure 20b, where a semicircle shaped low velocity field appears at the left and in the same y-axis coordinates as the input.

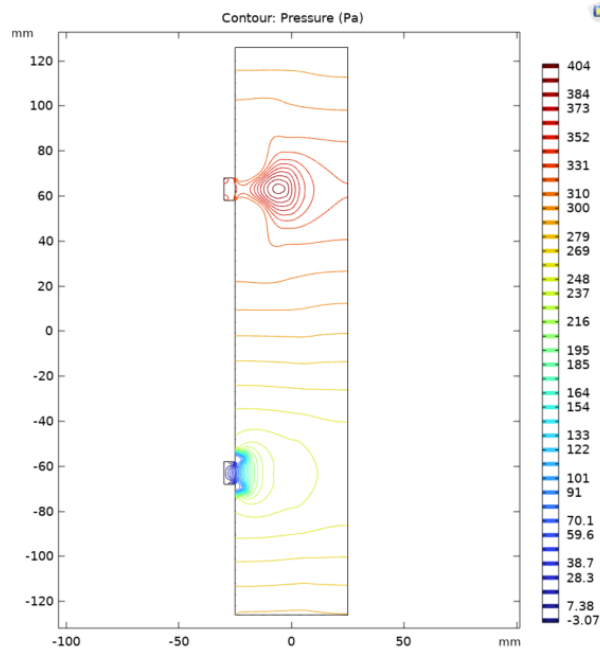


Figure 21: Pressure map of the design domain

### 3.1.3 Multi-physics Problem

Once the single physics problems of temperature and fluid flow have been studied individually. A combination of the two is prepared to conduct the multi-physics study. The same geometry with the same conditions as defined in figure 12 however, the uniform heat generation changes from a volumetric heat rate,  $Q$ , of  $10 \frac{W}{m^3}$  to a heat power input of 100 W. In COMSOL this is translated into volumetric heat rate through the formula  $\frac{P}{V}$ , where the volume is calculated from the defined surface domain and out of plane thickness of 0,01m. As well as the previous single physics problems, the MMA algorithm and the SIMP interpolation scheme are used. However in this case the initial value of  $\gamma$  is set to 1.

#### Governing equations

The steady state governing equations for an idealized porous medium are the virtually the same as in the the ones defined in section 3.1.2, and are:

$$\begin{cases} \rho \cdot (u \cdot \nabla)u = -\nabla p + \mu(\nabla^2 u) + \alpha(\gamma)u \\ \rho \cdot (\nabla)u = 0 \end{cases} \quad (3.13)$$

Where the first element describes the Navier-Stokes fluid flow and the second defines

the incompressibility of the fluid.  $\rho$  refers to the density of the fluid, and  $\eta$  the dynamic viscosity. And where  $\alpha$  is the inverse permeability and  $u$  is the velocity field vector.

Additionally, the equation that governs the steady state convection-diffusion heat transfer, where  $Q$  is the uniform heat generation,  $C$  the heat capacity and  $k$  represents the and thermal conductivity, is as follows:

$$\rho C(u \cdot \nabla T) = \nabla \cdot (k \nabla T) + Q \quad (3.14)$$

### Objective function

The objective function for this optimization problem has two components that add together the heat transfer and fluid flow in one common equation. The general structure of this function is like this:

$$A = \omega_1 B + \omega_2 C \quad (3.15)$$

Where  $B$  is the thermal part of objective function and  $C$  is the fluid flow part. With  $\omega_1$  and  $\omega_2$  being weighting factors, set manually to simplify the process, that scale the two objective functions that compose  $A$ , and help tune the sensitivity of the objective function to either the thermal or fluid flow problem and assist in convergence. The objective functions  $B$  and  $C$  are defines as follows:

$$B = \int_{\Omega} (T - T_{in})^2 d\Omega \quad (3.16)$$

$$C = \int_{\Omega} \left[ \frac{1}{2} \eta \sum_{i,j} \left( \frac{\partial u_i}{\partial x_j} + \frac{\partial u_j}{\partial x_i} + \sum_i \alpha(\gamma) u_i^2 \right) \right]^2 d\Omega \quad (3.17)$$

This objective functions can be simplified. The thermal objective function,  $B$ , is equivalent to the mean temperature of the design domain for a constant heat generation, while the term  $C$  can be also interpreted as the total flow power dissipation inside the domain, or the pressure difference between the inlet and the output points. The resulting formulation of the multi-physics problems is:

$$\left\{ \begin{array}{l} \text{Find : } \gamma \\ \text{Minimizing : } A = \omega_1 (T_{avg,\Omega}) + \omega_2 (p_{in} - p_{out}) \\ \text{Subjected to:} \\ \rho \cdot (u \cdot \nabla) u = -\nabla p + \mu(\nabla^2 u) + \alpha(\gamma) u \\ \rho \cdot (\nabla) u = 0 \\ \rho C(u \cdot \nabla T) = \nabla \cdot (k \nabla T) + Q \\ \int \gamma d\Omega_d - V_{max} \leq 0 \\ 0 \leq \gamma \leq 1 \\ \text{Given : } k_{\gamma} = (0,001 + 0,999\gamma^{p_{simp}}) k_{max} \end{array} \right. \quad (3.18)$$

### Objective Function Selection

For evaluation and comparison, four different optimizations have been carried out with two different objective functions applied to two different volumetric factors of 0,3 and 0,5. The objective functions used are:

$$A_1 = B + 0,001C \quad (3.19)$$

$$A_2 = B + 0,01C \quad (3.20)$$

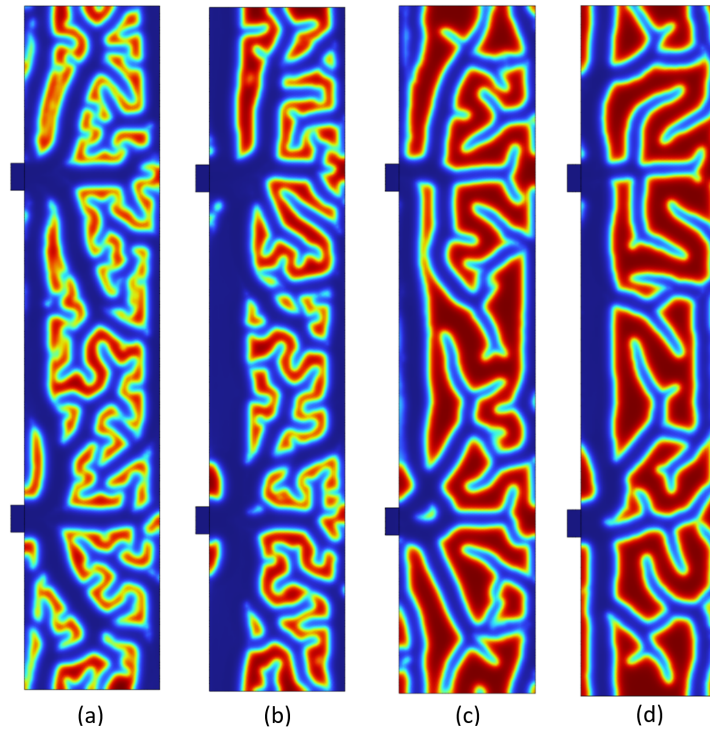


Figure 22: Topology optimization results of material distribution

In figure 22 a comparison of the material distribution for each of the four evaluation is presented. Figures (a) and (b) correspond to the results of  $A_1$  and  $A_2$  respectively for a volumetric factor of 0,3; while for a volumetric factor of 0,5, (c) is the solution of  $A_1$  and (d) is the solution of  $A_2$ .

- $V_{target} = 0,3$

In figure 23 the surface temperature maps of the objective functions are presented. Since the objective of the simulation is to lower the temperature of the domain to the minimum, the solution presented by the objective function  $A_1$  is the best in this regard, given that the maximum temperature in the domain is 297 K while for  $A_2$  the maximum temperature is 301 K. However, since the pressure drop is also taken into account in the objective functions, the results in minimization of pressure loss must also be analyzed.

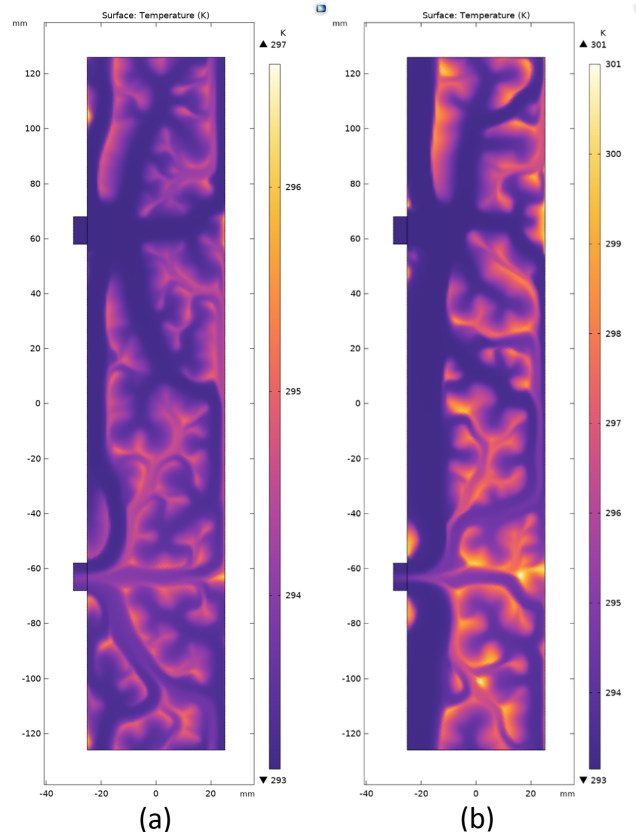


Figure 23: Domain temperature maps for volumetric factor of 0,3: (a)  $A_1$ , (b)  $A_2$

In the multi-physics objective functions, the pressure objective weighting factor is valued tenfold in the case of  $A_2$  compared to  $A_1$ . The results however are not proportional to the weighting factor applied. Being true that the pressure differential between the input and the output is higher in the solution for objective function  $A_1$ , it is only by 258 Pascals, as can be calculated by the values in figure 24. A reason for the rise in pressure differential for  $A_1$  can be observed in figure 25. Considering that the maximum flow speed is virtually identical, in (a) the main channel of circulation is smaller and experiences higher flow speeds, moreover, the water is conducted through more channels and is forced to travel a greater distance and higher speeds.

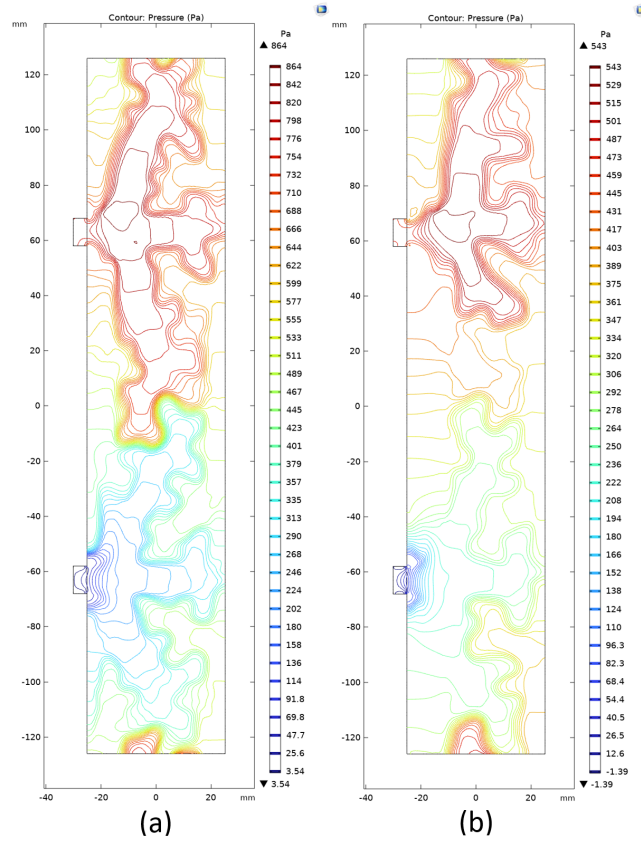


Figure 24: Domain pressure maps for volumetric factor of 0,3: (a)  $A_1$ , (b)  $A_2$

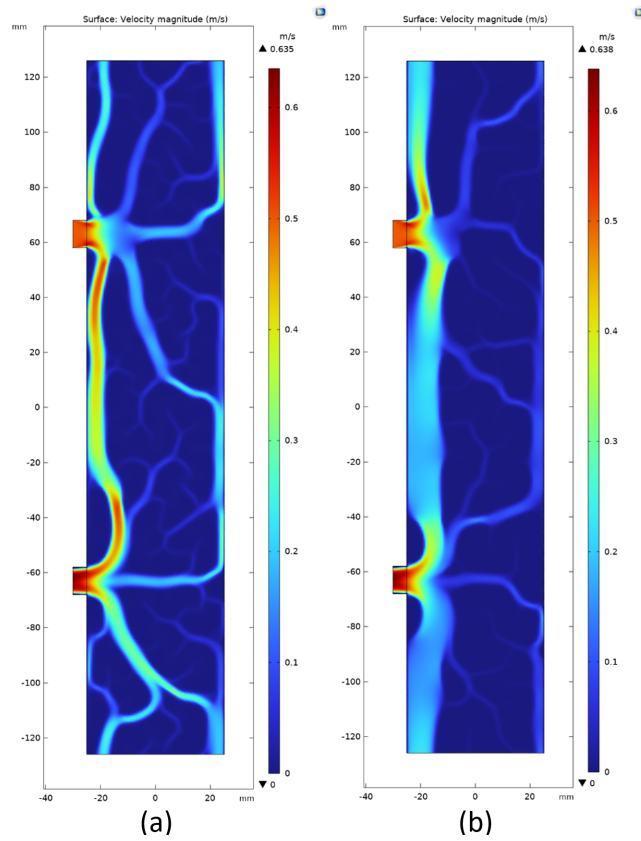


Figure 25: Flow velocity in the domain for volumetric factor of 0,3: (a)  $A_1$ , (b)  $A_2$

■  $V_{target} = 0,5$

As can be expected and show in figure 22, due to the higher volumetric factor, the presence of solid material calculated by the objective functions has increased in comparison to the result with volumetric factor equal to 0,3. An although differences can be found between the two results: (c) for  $A_1$  and (d) for  $A_2$ . A characteristic found in both is the presence of bigger and continuous solid formations and an flow dead ends, specially clear in figure 22d.

Form figure 26 can be observed that the temperatures of the solutions for the objective functions ((a) $A_1$ , (b) $A_2$ ) are in this case higher than the values registered in figure 23. Form the temperature values observed, the better solution is the one offered by objective function  $A_1$ . Not only is the median temperature lower, but also the hotspot temperature, 300 K compare to 323K for the solution of objective function  $A_2$ , but also the temperature distribution is more uniformed; while the temperature in the second case is concentrated in small local points.

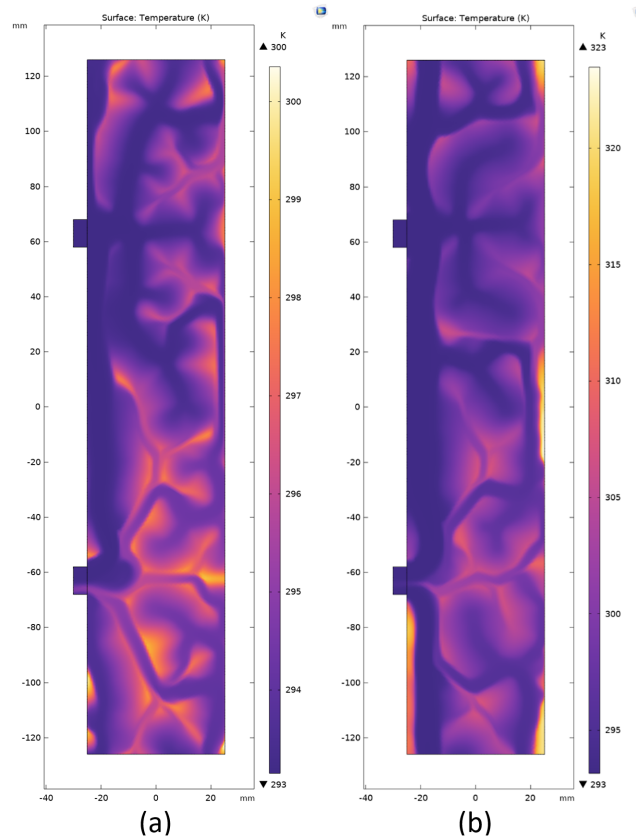


Figure 26: Domain temperature maps for volumetric factor of 0,5: (a)  $A_1$ , (b)  $A_2$

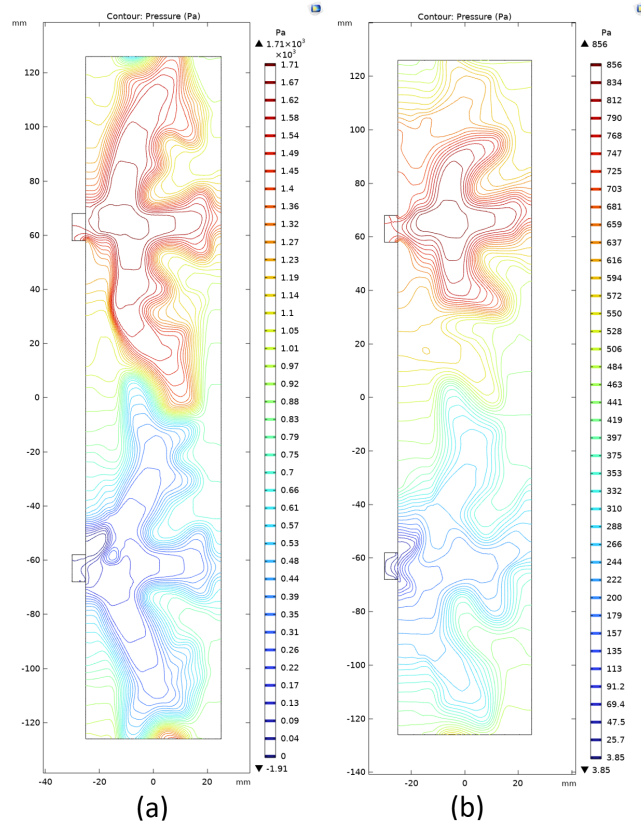


Figure 27: Domain pressure maps for volumetric factor of 0,5: (a)  $A_1$ , (b)  $A_2$

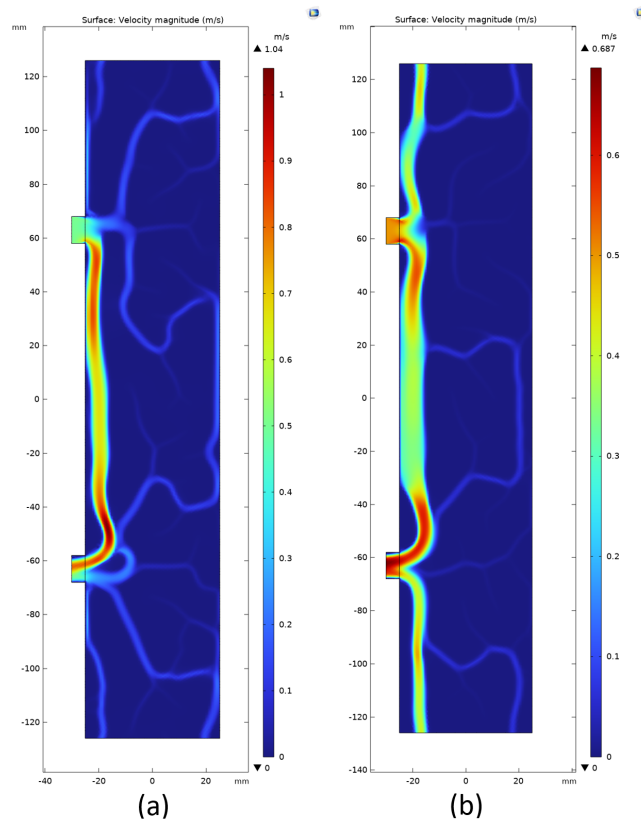


Figure 28: Flow velocity in the domain for volumetric factor of 0,5: (a)  $A_1$ , (b)  $A_2$

A product of the higher volumetric factor is the increase in pressure differential when compared to the results in figure 24. With again, notable differences in the results of  $A_1$  and  $A_2$ , being the drop lower in the later. This may be a product of the higher presence of solid material, which as observed in (figure 28a) can push flow speeds to a maximum of 1,04 m/s, while for the other simulations, the top flow speed doesn't exceed 0,69 m/s.

With all solutions analyzed and compared, the one found to be the optimal is the given for the objective function  $A_1$  with a volumetric factor of 0,3. Event though the pressure drop in the domain in the third best, only 8 Pa higher than the objective function  $A_2$  for volumetric factor 0,5, the temperature drop in the domain for this simulation is the lowest of all.

However this solution is not final, once the best objective function has been defined, further evaluation just be carried out with different initial values of  $\gamma$ .

### 3.1.4 Results with different initial gamma values

As stated in section 2.6, gradient based techniques maximum or minimum solutions are heavily dependant of the initial values of the optimization because the algorithm tends to converge on closest maximum or minimum to the inital point. Since the calculations to determine the objective function were all carried out using the same initial values of  $\gamma_i = 1$ . Further optimizations using the defined objective function  $A_1$  were undertaken with different initial values to ensure the final solution was the absolute minimum. Since a solution for an initial value of 1 is already available, testing was carried out using the following initial values: 0,1; 0,3; 0,5; 0,7. It must be pointed out that the solution for  $\gamma_i = 0,1$  the calculation process return an erroneous solution and is therefore not included in this study.

#### Comparisons between results

As can be observed in figure 29, the four different tests return solutions with comparatively similar overall geometries. The presence of a five channel ramification from both input and output can be observed in all solutions. Other common features include the presence of a solid element opposite to the input channel. Although the size and geometry of this feature greatly varies depending on thee initial value, with the solution for  $\gamma_i = 0,5$  being connected to a serpentine feature that extends horizontally, normally disconnected in the other solutions; and the solution for  $\gamma_i = 0,3$  presenting a material connection between the solid material in front of the input channel and the material at the top, which is not present in the rest of solutions. Also close to the input, and in both sides, is the presence of a quasi S-shaped body with an elongated tail that extends to the input channel and is responsible for designing some of the channels that originate form the input. This feature is however more extent in the solution for  $\gamma_i = 1$  since it connects to another feature on the left most point, elongating it significantly to the other solutions, specially the one for  $\gamma_i = 0,7$ . Two last feature

common to all results are the presence of two bodies next to the output that tend to develop a tail away from the output, this is specially significant for  $\gamma_i = 1$ .

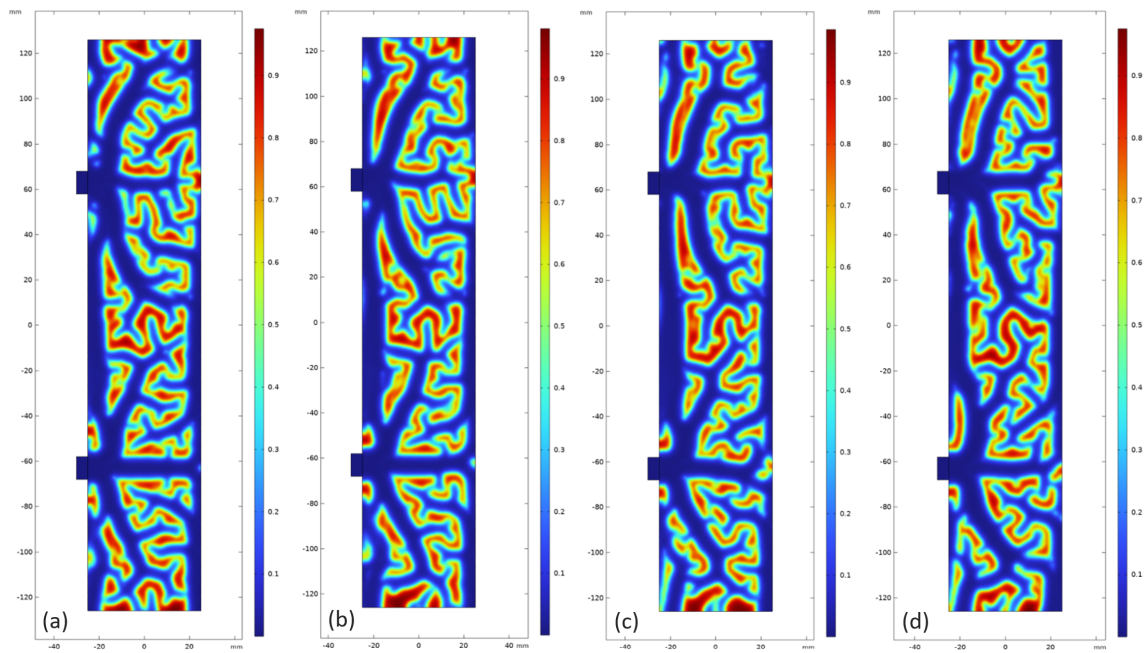


Figure 29: Material distribution for: (a)  $\gamma_i = 0,3$ ; (b)  $\gamma_i = 0,5$ ; (c)  $\gamma_i = 0,7$ ; (d)  $\gamma_i = 1$ ;

When it come to temperatures resultant in each solution, no big differences can be found. Having to resort to check the centesimal point to find any differences. With this precision, it can be concluded that the average temperatures are basically identical in all four cases and the maximum temperature is lowest for  $\gamma_i = X$ . This will be the solution selected for the construction of the 3D model and the comparison with the traditional solutions.

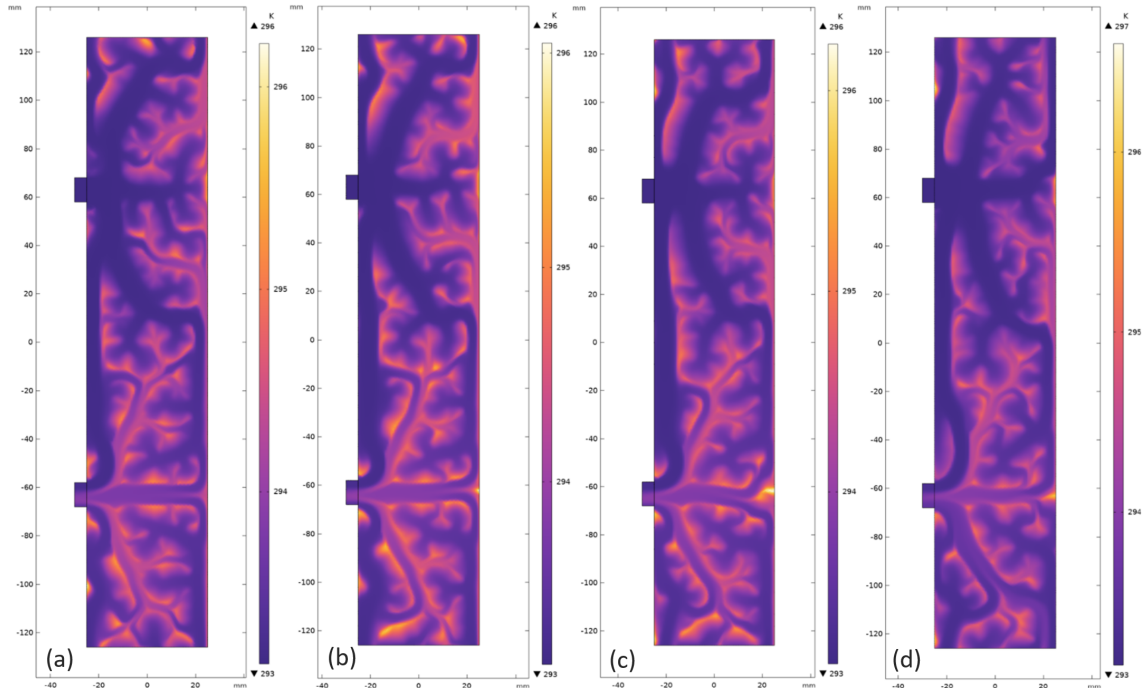


Figure 30: Domain temperatures for: (a)  $\gamma_i = 0,3$ ; (b)  $\gamma_i = 0,5$ ; (c)  $\gamma_i = 0,7$ ; (d)  $\gamma_i = 1$ ;

Table 4: Temperature results for different  $\gamma_i$

$\gamma_i$	0,3	0,5	0,7	1
Avg. $T$ (K)	293,77	293,78	293,78	293,78
$T_{max}$ (K)	296,21	296,05	296,23	296,60

Observing the absolute value of the fluid flow speed helps to understand where circulation is higher and also understand where the patches where temperature is highest may arise. Constant circulation of water at reasonable speeds is necessary to ensure proper heat evacuation. For the central section of the domain of every solution, where the S-shaped geometry is present, two clear main flow paths are present, one that goes directly from the input to the output and another that traverses diagonally to the right edge until contacting the midpoint between the input and the output, from there it continues parallel to the right edge until it contacts the output and turns 90 degrees to face it. This can be observed in all solutions and is related to the 5-prong division of the flow forced by the geometry. However, for the solution of  $\gamma_i = 1$ , one of the channels extends in a straight line until it contacts the right edge of the geometry and then turns 90 degrees to flow parallel to the right edge.

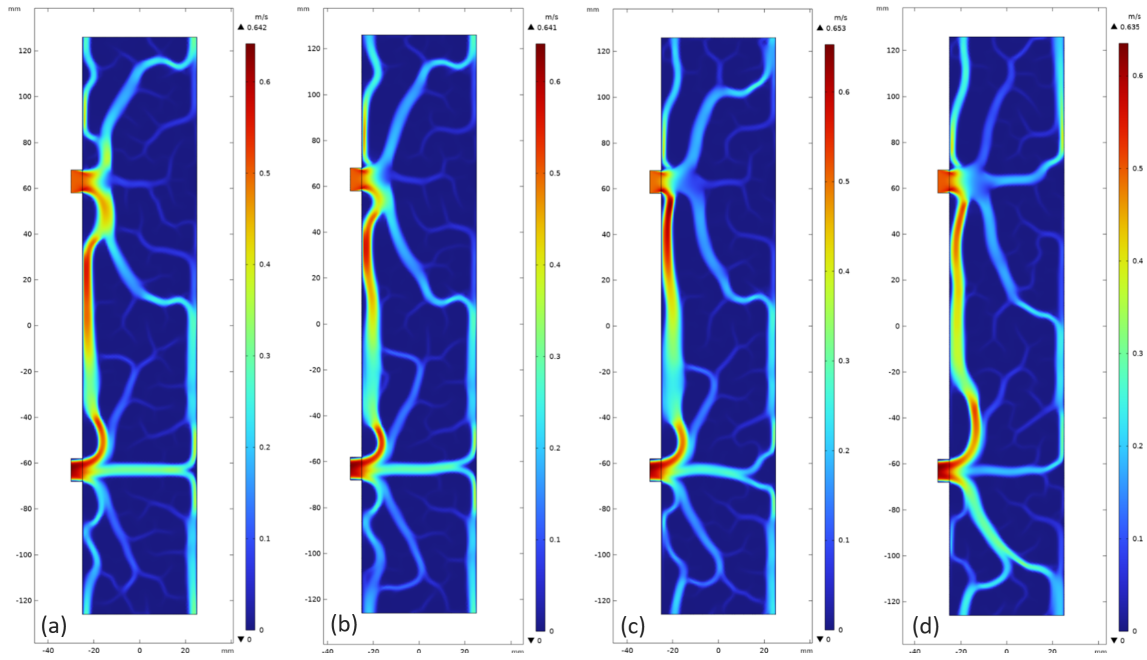


Figure 31: Absolute velocities inside the domain for: (a)  $\gamma_i = 0,3$ ; (b)  $\gamma_i = 0,5$ ; (c)  $\gamma_i = 0,7$ ; (d)  $\gamma_i = 1$ ;

### Selected solution

The selected solution is the one resulting from  $\gamma_i = 0,5$ . Since it is the resulting geometry that achieves the lowest hotspot temperature, 296,05 K, and average temperature, 293,78 K; as presented in table 4. Moreover, as shown in figure 31, this geometry doesn't present any serious disadvantage in regards to fluid flow distribution it's velocity inside the domain.

## 4. COMPARISON OF SELECTED DESIGN WITH TRADITIONAL SOLUTIONS

### 4.1 Traditional solutions models

In order to put the solution design performance into context, a comparison against traditional water jacket designs has been performed. For this case, three different designs are selected: an spiral, U-shaped and coaxial.

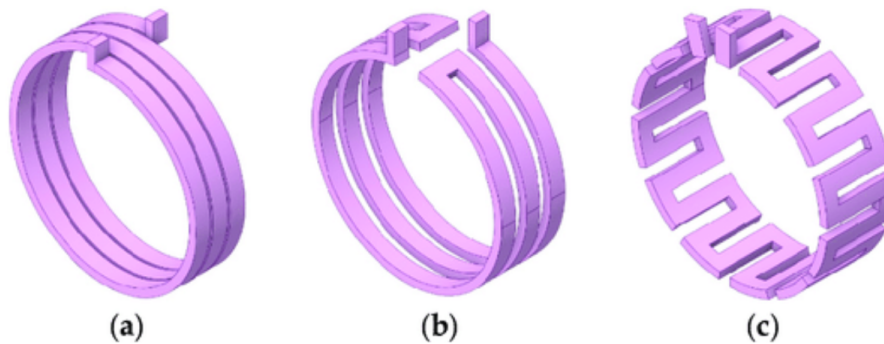


Figure 32: Traditional water jacket designs: (a)Spiral, (b)U-shaped, (c)Coaxial [91]

The designs realized to be tested follow the same structure as the ones showed in figure 32. With the spiral and U shaped designs having the input and output on opposite side of the heat exchanger, while the coaxial design has them side to side in the same cylinder surface. The three designs have an inner diameter of 80 mm and length of 50 mm to reassemble in dimensions to the topology optimized solution, as well as a squared channel cross section of 10 mm with cylindrical input and output pots of the same diameter as the square edge. This dimension similarities as well as the port dimensions are chosen to be able to allow for comparison with same dimensions and mass flow in all tested designs.

For this comparison study 3D models of the four different designs, the three showed in figure 32 plus the solution design of the study, are subjected to a thermal source in the inner surface of the cylinder while having water flowing on the interior.

### 4.2 Proposed solution model

The final solution from the optimization analysis from chapter 3 is the one composed by the objective function for a volumetric factor of 0,3:

$$A_1 = B + 0,001C \quad (4.1)$$

The 3D model of the result for this objective function, figure 33 has been realized following the material distribution shown in figure 29(b), and is represented in the following figure:

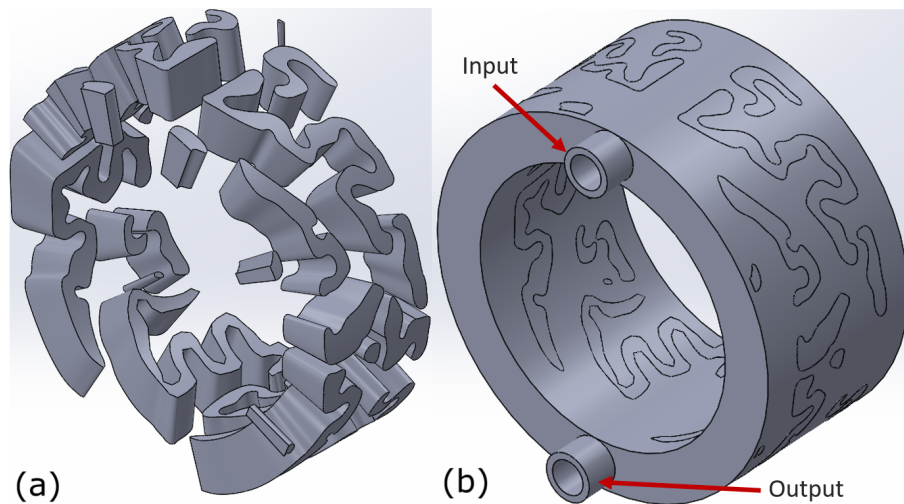


Figure 33: 3D model of selected result: (a) Model of the result on the interior of the water jacket; (b): Water jacket model exterior showing input and output ports

#### 4.2.1 Testing parameters

In the first instance, the thermal load and fluid flow speed were set to the same parameter as in the 2D study. Flow speed at the input of 0,5 m/s with a fluid temperature of 293,15 K, and heat power input of 100 W in the inner cylindrical surface. However, when the initial test was carried out the resulting values for were too close together, as in the case of the evaluation of the 2D models. For this reason, the heat power input into the inner surface of the cylinder was elevated to 200W. This allowed for more easily discernible discrepancies.

#### 4.2.2 Results for the spiral design

For the spiral shaped water jacket the maximum temperature has been registered at 295,69 K. With the majority of the highest temperatures registered in the geometry where no water channel is present, seen in the lower left part of the inner cylinder surface in figure 34(a) and with also higher temperatures, although not close to the maximum in the channel-less part, next to the input region. Interestingly, the inner cylinder surface experiments higher temperatures in the sections where it runs parallel to the inner flow channel edge, than the sections where aluminium connects the inner surface to the outer surface of the cylinder, s seen in figure 34(b). This is caused by differential o temperature, since as also shown in (b), the inner surface of the flow channel is at the same temperature of the inner surface of the cylinder.

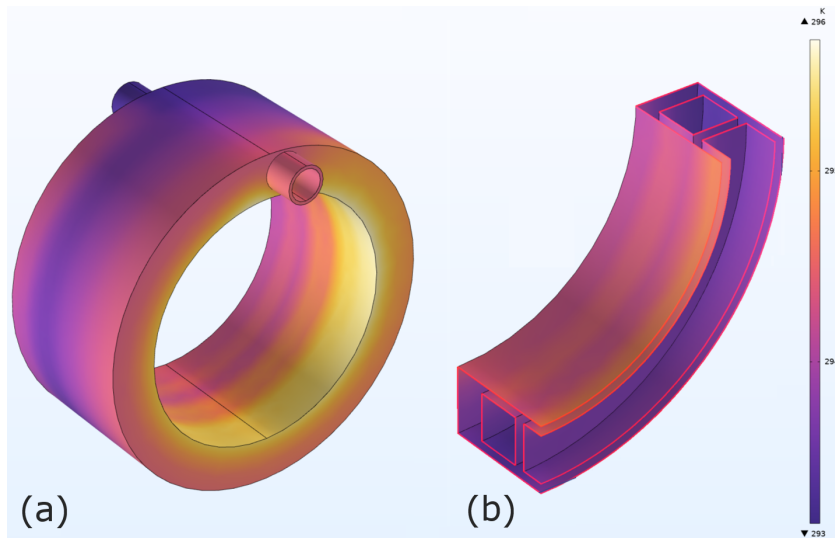


Figure 34: Spiral design: (a) Water jacket temperature, (b) Cross section of water jacket

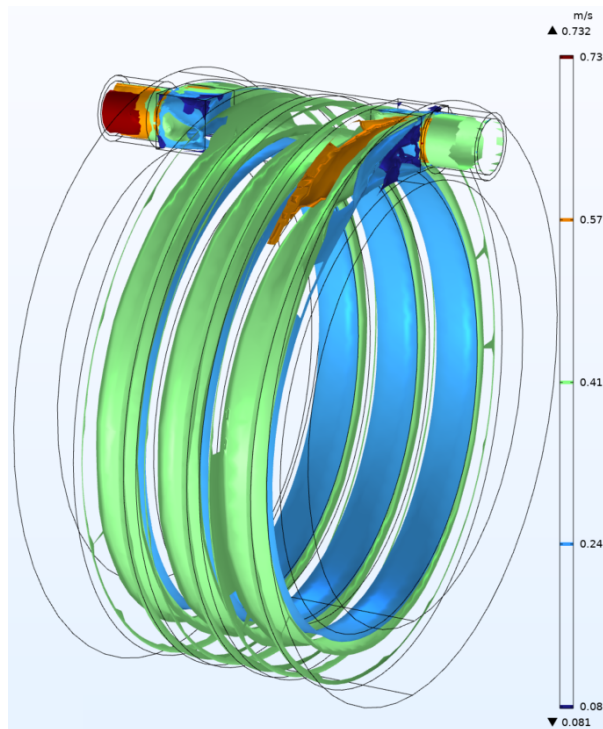


Figure 35: Speed of the flow inside the channels for the spiral design

However in the sections where aluminum is present, more material is available to absorb with parallel flow channel surfaces that effectively double the available cooling surface. Another factor that contributes to this phenomenon is the flow speed; since flow is slower in the surface of the inner flow channel edge than in the other edges perpendicular to it as shown in figure 35.

### 4.2.3 Results for the coaxial design

The maximum temperature registered for the coaxial design is 296,25 K. As in the same case as the previous analysis, higher temperatures are registered in the sections of the inner cylinder surface, where the inner flow channel edge runs closely parallel to it and with a very small temperature differential, visible in figure 36(b). Moreover, in this same figure, higher temperature can also be observed in the outer surface of the cylinder in the aluminum filled sections, presenting the opposite tendency than in the inner surface. It can be concluded that the aluminum conducts the heat generated in the inner surface to the exterior of the body, while the water flowing in the channels, uses inner edge of the and the vertical walls to absorb thermal energy from the aluminum. In figure 36(b) the increase in temperature in the vertical walls is visible, specially in the top left corner of the figure.

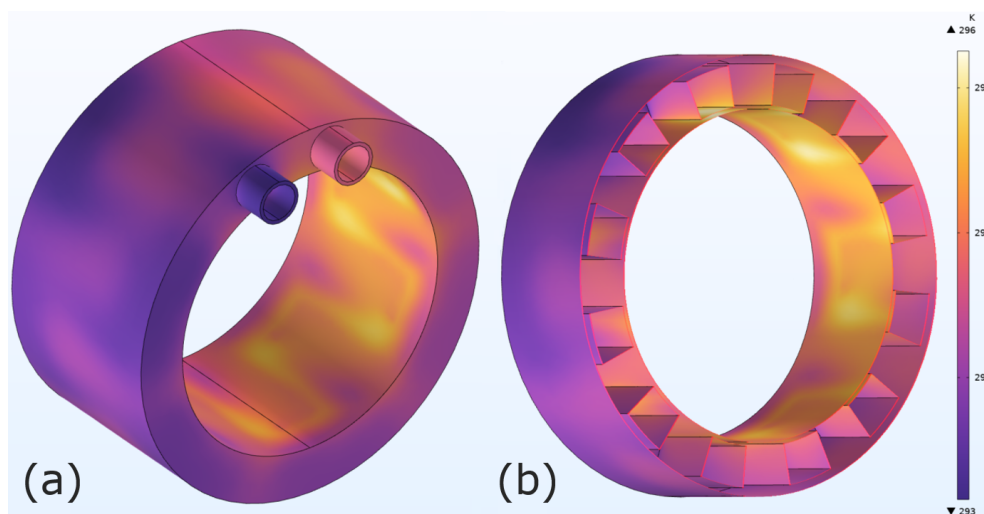


Figure 36: Coaxial design: (a) Water jacket temperature, (b) Cross section of water jacket

With figure 37 and figure 36 it can be observed that cooler temperatures both on the outer and inner surfaces of the cylinder are directly related to a faster flow. As well as a lower temperature in the top and lower surfaces of the cylinder, for which the thinner aluminum body and a fast flow of water allow for higher thermal energy extraction.

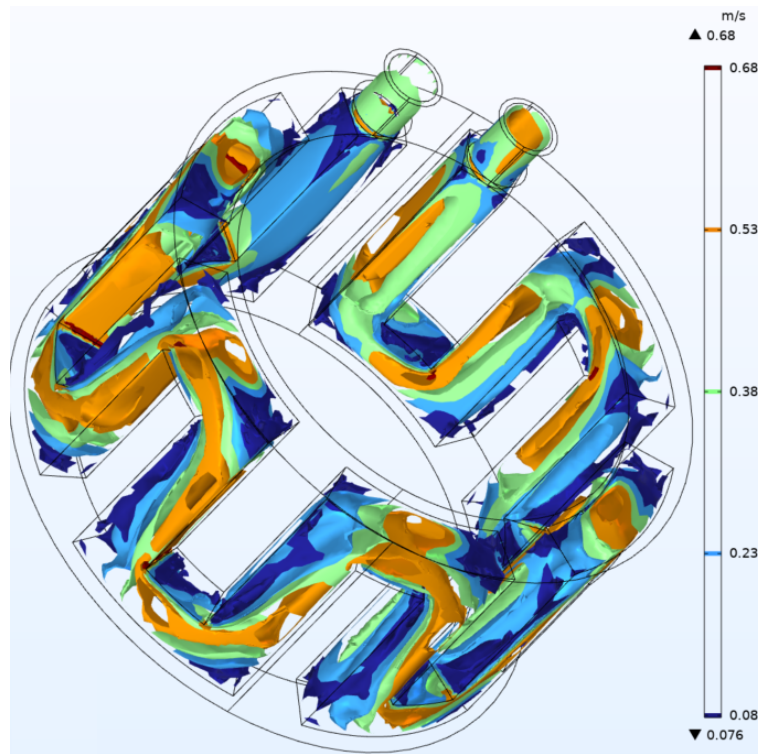


Figure 37: Speed of the flow inside cooling channels of the coaxial water jacket

#### 4.2.4 Results for the U-shaped design

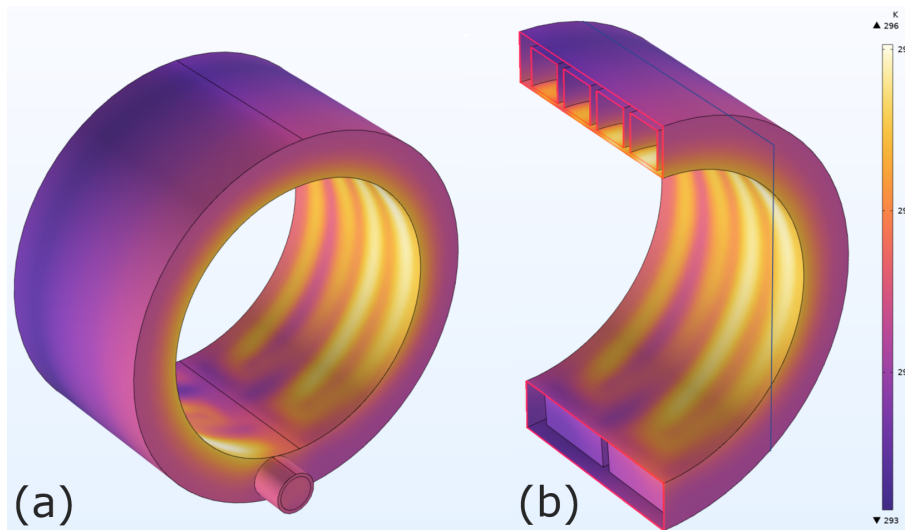


Figure 38: U-shaped design: (a) Water jacket temperature, (b) Cross section of water jacket

The U-shaped designed water jacket presents a maximum temperature of 296,03 K. For this design however, a lot of the inner surface of the cylinder presents temperatures very close to the domain maximum. As well as in the previous designs analyzed, these temperatures are located in the inner surface of the cylinder and along

the flow channels from the water, with increasing values the greater the distance from the input.

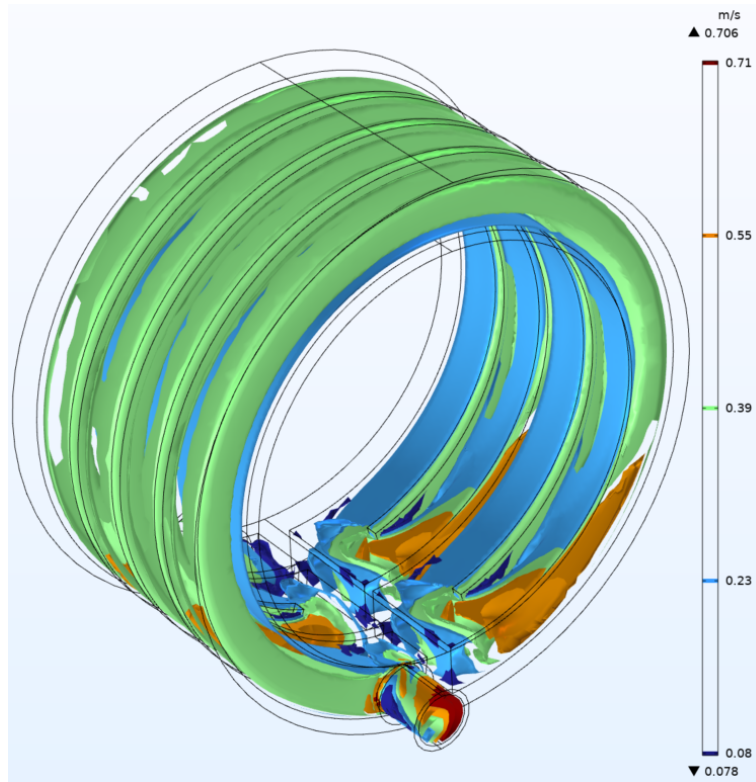


Figure 39: Speed of the flow inside cooling channels of the U-shaped water jacket

However, as observed in figure 38, unlike the coaxial design the distribution of temperature in the outer surface increases progressively and doesn't present acute temperature differentials. However this may result in a higher average surface temperature for the inner cylinder face that would negatively affect the performance of the water jacket. However with an average temperature of the inner cylinder surface of 295,09 K, this seems unlikely.

In figure 39, the presence of high flow speed in the change of U-turns explains the increased cooling performance that can be located in part where it geometrically coincides with the thermal image presented in figure 38(a). There a lower temperature compared to the main body of the channel is observable provoked by higher flow speeds that are related to increased heat exchange rates.

#### 4.2.5 Results for the topology optimized design

The TO design developed in this study experiences a maximum temperature of the inner cylinder surface of 298,63 K. Again, as it can be observed in figure 40(a), the aluminum geometries on the interior of the water jacket carry the heat applied on the inner surface to the outer portions of the cooling channels, which takes bigger

advantage of the water flow; a characteristic also presented in figure 40(b), where higher temperatures can be observed in the outer more parts of the water flow. However, when comparing figure 40 and figure 41 side to side, more complete picture of the function of the design is presented. figure 41 presents sheds light to the fact that the flow speed is very reduced all across the geometry, except the locations in proximity to the input and the output. Moreover, some of the spaces of the geometry seem to not even present flow circulation. This explains the temperature results from figure 40.

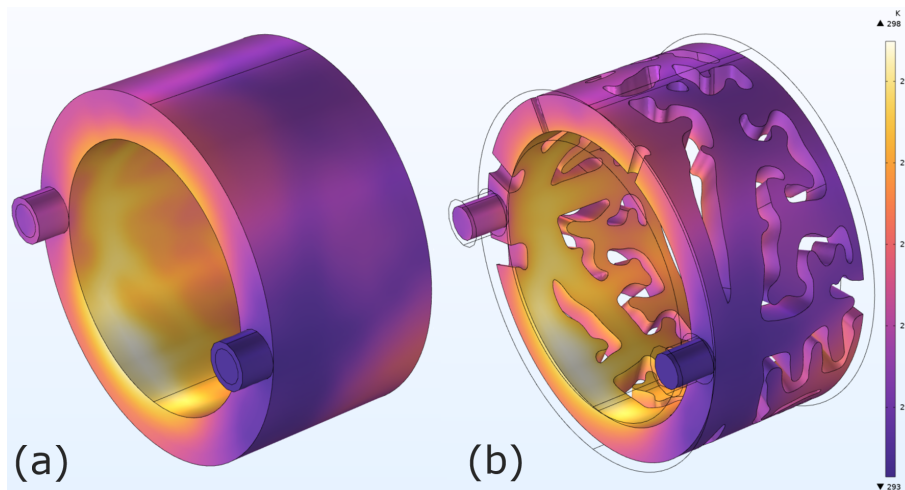


Figure 40: TO design: (a) Water jacket temperature, (b) Cross section of water jacket

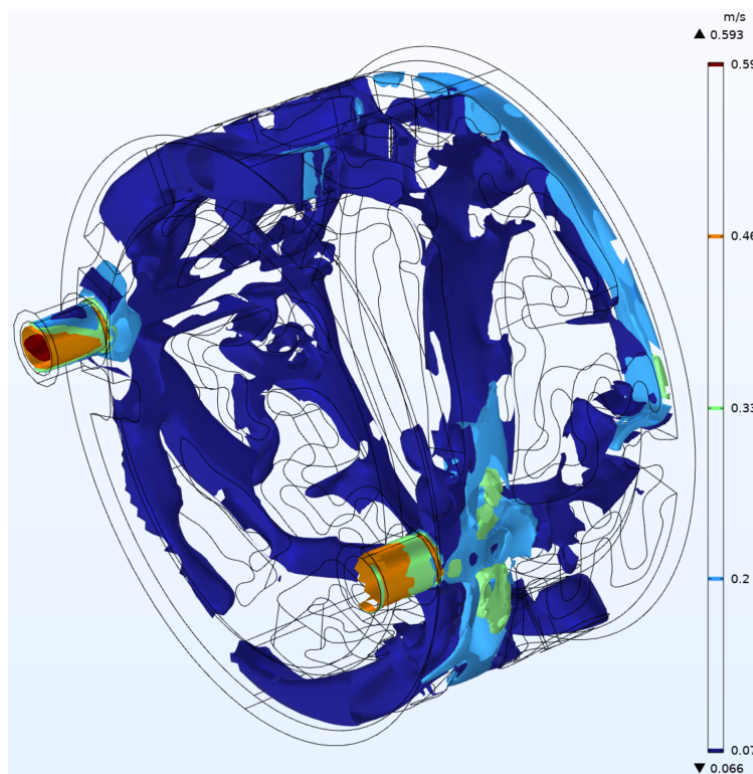


Figure 41: Speed of the flow inside cooling channels of the TO water jacket

Low water flow speed results in the water staying on a fixed point for longer period of time, and hence absorbing greater amounts of heat and therefore increases in temperature. This increase in temperature is translated in an accumulation of heat in the inner surface of the cylinder since hotter water has a lesser temperature differential with surrounding aluminum bodies, reducing heat flux. This effect is exacerbated the slower the flow presenting the maximum effect in the regions where the flow is basically stagnant.

### 4.3 Conclusions of the comparison

After the evaluation of the TO design realized in this study and models using traditional designs: spiral, coaxial and U-shaped. It can be concluded that the purpose of this work has failed, since the TO design is proven to be the worst solution of the four analyzed. In table 5, a comparison between the average and maximum temperatures is presented. The maximum surface temperature within the four designs is that of the TO solution, and while the three traditional solutions average temperature range between values of 294,78 K to 295,90 K; the average temperature value for the TO design is 296,49 K. Which clearly sets this heat exchanger apart. The same trend repeats for the maximum temperature for the inner surface, where the maximum temperature of the TO water jacket is set way higher at 298,63 K, when compared to the highest maximum temperature from the traditional designs, which is that of the Coaxial design, and has a value of 296,03 K. 2,6 K lower when compared to the TO design maximum temperature, but only 0,56 K higher than the lowest temperature, from the Spiral design. Therefore it is clear that the TO designed water jacket has the worst cooling performance out of the 4 designs evaluated.

Table 5: Average and maximum temperature in Kelvin for the four different designs evaluated

Design	Spiral	Coaxial	U-Shaped	TO
Avg. $T$ (K)	294,78	294,95	295,90	296,49
$T_{max}$ (K)	295,69	296,25	296,03	298,63

Furthermore, when comparing the design solution realized with the 2D model with the final design composed in 3D. Inconsistencies in the correlation between the model arise. For instance, during the 2D computational calculations for topology optimization, the problem of stagnant flow observed in various regions of the domain was not discernible. While true that the flow directions can be correlated, the velocity magnitude cannot, as it can be observed when comparing figure 31(b) to figure 41. One hypothesis that can explain the disparity may be found in the cross section of the channels to this regions of the geometry and the pressure in the vicinity.

A parameter that clearly represents that the design realized in this study was a failure is the thermal resistance. For the the topology optimized design this value was

0,024K/W while the average of the the three traditional designs was 0,012 K/W. Therefore, future work is required to amend the design and procedure.

Although the same simplified objective functions are used as the ones presented in Dede et al. [70], further indication is necessary, although it is considered to be the right track since in two more studies similar objective functions are applied [59, 92], with special attention paid to the second study where a similar solution becomes viable. Further work should also put into realizing more viable constraints. More work should be put into making sure that 2D and 3D models can correlate, this would simplify the calculations and reduce hardware requirements, a consideration that was undertaken for this approach in this work.

## 5. SUMMARY

The effective thermal management of electric machines is crucial to ensure a reliable and efficient function. Increased temperatures are associated to the enhanced losses due to increased resistivity of the conductor material in the windings, usually copper, through the following equation:  $\rho_T = \rho_0[1 + \alpha(T - T_0)]$ ; Where the base resistivity of the material  $\rho_0$  increases with the temperature  $T$ . Another relevant effect of is found in the insulator material, where an increase of 10 °C has been associated with a reduction in half of the insulator life.

To achieve correct thermal management of electrical machines, three types of cooling systems are used. The simplest one is passive air cooling. This type of cooling relies on natural convection to cool a surface, and presents limitations to the size of the cooling surface available and the pressure drop that interacted surfaces can produce, therefore reducing convection. To further enhance the performance of passive air cooling, the force induction of flow through a heat sink results in active air cooling. With this type of cooling, increased flow speed and circulation of mass allows for better cooling performances. Lastly, as the name indicates, liquid cooling makes uses of liquids to manage the temperature of electrical machines. Relevant to this study is the use of water jackets, cylindrical bodies that encapsulate the core of and electric machines, usually inner rotor electrical machines, with hollow channels carved between the outer and inner cylindrical surfaces to allow for the circulation of a liquid cooling agent, usually water. The water absorbs the heat generated by the electrical machine, reducing the maximum temperature it can active to later exchange the thermal energy with the air.

The shape of the channels inside the water jacket has relied until now in traditional shapes and geometries like the spiral, U-shapes and coaxial designs. However, the rise of additive manufacturing specially metal AM, with the ability to manufacture complex geometric designs; allows for realization for complex design geometries inside the water jacket volume that increase heat exchange capacity therefore increasing the efficiency of the heat exchange and further reducing the temperature of the electrical machine, with all the advantages. The complex designs can be realized using topology optimization. Which uses a objective function that include a component whose objective is to minimize the average temperature of the design domain while maintaining to the minimum the pressure drop of the flow. To ensure that the absolute minimum solution of the objective function found, different iterations of the calculations are undertake using different constraint values and initial parameters. To reduce the computational load, the model ah been developed in a 2D space and later translated to a 3D space for evaluation and comparison with other tradition designs.

The resulting topology optimized design from this work proved to be unsuccessfully in improving the thermal management performance when compared to the tradition designs (spiral, U-shaped and coaxial), with a thermal resistance considerably higher (0,024 K/W) when compared to the lowest thermal resistance of the three traditional

design tested, the spiral design with values of (0,012 K/W). In the posterior analysis, the reduced performance of the TO design is attributed to the lack of water flow and the very reduced water flow speed in various part of the geometry generated by the result of the objective function.

The conclusion of this study is therefore, that the application of TO for the design optimization of heat ex changers is viable. However, further investigation of the applied objective, in this case:  $A_1 = B + 0,001C$  with the  $B$  component being the objective function that reduces the average temperature of the design domain; and  $C$  being the component that reduces the pressure differential between input and output and the constraints that govern the final achieved result must be undertaken to achieve a design solution that better manipulates water flow. The constraints must also be revised. While the constraint that limits the maximum volume that solid material covers relative to the total volume of the domain works as intended, further constraint must be considered that may impose minimum flow requirements. With all this future work would also involve the actual production of a successful design using metal AM to further certify the performance of the simulations.

## 6. KOKKUVÕTE

Elektrimasinate tõhus jahutamine on oluline usaldusväärse ja efektiivse töö tagamiseks. Kõrgemad temperatuurid on seotud mähistes oleva juhtiva materjali, milleks on tavaliselt vask, suurenenud takistusega, mis tuleneb järgnevast võrrandist:  $\rho_T = \rho_0[1 + \alpha(T - T_0)]$  - kus materjali algtakistus  $\rho_0$  suureneb temperatuuriga  $T$ . Teine oluline mõju on seotud isoleeriva materjaliga, kus 10 °C suurenemisega on seostatud isolatsiooni eluea vähenemine poole võrra.

Elektrimasinate jahutamiseks kasutatakse kolme tüüpi jahutussüsteeme. Lihtsaim neist on passiivne õhujahutus, mis kasutab pinna jahutamiseks loomulikku konveksiooni, kuid sel juhul on kasutatav jahutuspind piiratud rõhulangu poolt. Passiivse õhujahutuse jõudluse parandamiseks sooritatakse sundkonveksiooni läbi soojusvaheti, mille tulemuseks on aktiivne õhkjahutus. Seda tüüpi lahendusega võimaldavad suurenenud voolukiirus ja õhumassi transport paremat jahutust. Viimaks, nagu nimigi ütleb, kasutatakse vedelikujahutust elektrimasinate temperatuuri alandamiseks. Selles töös on uurimise all veemantlid ehk silindrilised kehad, mis ümbritsevad sisemise rootoriga elektrimasina südamikku, mille sisse on kujundatud tühjad kanalid, et võimaldada vedeliku, tavaliselt vee, tsirkulatsiooni. Vesi neelab elektrimasinast tekkinud soojust, vähendades selle maksimaalset temperatuuri, mille ta hiljem saab vahetada õhuga läbi välimise radiaatori.

Kanalite kuju veemantlis on seni toetunud traditsioonilistele geomeetriaale nagu spiraal, U-kujulised ja koaksiaalsed kujundid. Siiski, kihtlisandusmeetodite tõus, eriti metalli 3D-printimine, võimaldab keerukate geomeetriaale realiseerimist veemantli sisemuses, mis suurendab soojusvahetuse võimekust ja seeläbi efektiivsust, parandades elektrimasina temperatuuri veelgi. Komplekssed kujundid saab luua läbi topoloogiaoptimeerimise (TO). See kasutab sihtfunktsiooni, mis sisaldab komponente eesmärgiga minimeerida kavand-domeeni keskmist temperatuuri, säilitades minimaalse rõhulanguse. Selleks, et tagada sihtfunktsiooni absoluutne miinimum, viiakse läbi iteratiivsed arvutused, kasutades erinevaid piir- ja algväärtusi. Arvutuskoormuse vähendamiseks on mudel arendatud 2D-ruumis ja hiljem teisendatud 3D-ruumi, eesmärgiga seda hinnata ja võrrelda tavapäraste kujunditega.

Selle töö tulemusena saadud topoloogiaoptimeeritud disain osutus ebaõnnestunuks jahutuse jõudluse parandamisel võrreldes tavapäraste kujunditega (spiraal, U-kujuline ja koaksiaalne), olles soojustakistuselt märkimisväärselt kõrgem (0,024 K/W) võrreldes kolme traditsioonilise kujundiga, millest kõige madalama soojustakistusega oli spiraalikujund (0,012 K/W). Lõplikus analüüsis omistatakse TO disaini vähenev jõudlus tugevalt vähenenud voolukiirusele erinevates jahuti osades objektiivfunktsiooni põhjal genereeritud geomeetrias.

Seega järeldub antud uuringust, et TO rakendamine soojusvahetite kuju optimeerimiseks sisaldab potentsiaali. Siiski tuleb teha täiendavaid uuringuid sihtfunktsiooni, antud juhul:  $A1 = B + 0,001C$ , osas, kus B komponent on domeeni keskmist tem-

peratuuri käsitlev, ja C komponent käsitleb sisse- ja väljundvahelise rõhuvahe minimeerimist. Samuti tuleb üle vaadata piirtingimused. Kuigi kavand-domeeni maksimaalse täiteteguri piirang töötab ootuspäraselt, peab looma uued piirangud, mis garanteeriks minimaalse veevoolu koguse. Koos kõige sellega sisaldaks tuleviku töö ka füüsilise prototüübi valmistamiseks läbi metalli 3D-printimise, et kinnitada simulatsioonide tulemused.

## Bibliography

- [1] Rong Yang et al. "Analysis of an IPM machine with grain boundary diffusion processed magnets". In: *8th IET International Conference on Power Electronics, Machines and Drives (PEMD 2016)*. 2016, pp. 1–6. DOI: 10.1049/cp.2016.0247.
- [2] Kevin Bennion, Justin Cousineau, and Gilbert Moreno. *Electric motor thermal management for electric traction drives*. National Renewable Energy Laboratory, 2015.
- [3] Hamid A Toliyat and Gerald B Kliman. *Handbook of electric motors*. Vol. 120. CRC press, 2018.
- [4] European Commission et al. *Study on energy subsidies and other government interventions in the European Union – Final report – 2023 edition*. Publications Office of the European Union, 2023.
- [5] Dmytro Konovalov et al. "Recent Developments in Cooling Systems and Cooling Management for Electric Motors". In: *Energies* 16.19 (2023). ISSN: 1996-1073.
- [6] Rafal Wrobel. "A technology overview of thermal management of integrated motor drives – Electrical Machines". In: *Thermal Science and Engineering Progress* 29 (2022), p. 101222. ISSN: 2451-9049.
- [7] T.A. Lipo. *Introduction to AC Machine Design*. IEEE Press Series on Power and Energy Systems. Wiley, 2017. ISBN: 9781119352167.
- [8] David A. Staton and Andrea Cavagnino. "Convection Heat Transfer and Flow Calculations Suitable for Electric Machines Thermal Models". In: *IEEE Transactions on Industrial Electronics* 55.10 (2008), pp. 3509–3516.
- [9] Anibal Valenzuela and Juan Tapia. "Heat Transfer and Thermal Design of Finned Frames for TEFC Variable-Speed Motors". In: *Industrial Electronics, IEEE Transactions on* 55 (Nov. 2008), pp. 3500–3508.
- [10] G.M. Gilson et al. "A combined electromagnetic and thermal optimisation of an aerospace electric motor". In: Oct. 2010, pp. 1–7. DOI: 10.1109/ICELMACH.2010.5607893.
- [11] Cassiano Cezario and Amir Oliveira. "Electric motor internal fan system CFD validation". In: Oct. 2008, pp. 1–6.
- [12] Yew Chuan Chong. "Thermal analysis and air flow modelling of electrical machines". PhD thesis. June 2015.
- [13] Yaohui Gai et al. "Cooling of Automotive Traction Motors: Schemes, Examples, and Computation Methods". In: *IEEE Transactions on Industrial Electronics* 66.3 (2019), pp. 1681–1692.
- [14] Yew Chuan Chong. "Thermal analysis and air flow modelling of electrical machines". PhD thesis. June 2015.
- [15] Pavel Ponomarev, M. Polikarpova, and J. Pyrhönen. "Thermal modeling of directly-oil-cooled permanent magnet synchronous machine". In: Sept. 2012, pp. 1882–1887. ISBN: 978-1-4673-0143-5.

- [16] Yanzhu Jin et al. "Design of Low-Pressure Sand Casting Process for Water-Cooled Motor Shell in Electric Vehicle". In: *Journal of Physics: Conference Series* 2101 (Nov. 2021), p. 012052.
- [17] Roman Pechanek and Lukas Bouzek. "Analyzing of two types water cooling electric motors using computational fluid dynamics". In: Sept. 2012, LS2e.4-1. ISBN: 978-1-4673-1970-6.
- [18] Christian Kral, Anton Haumer, and Thomas Bäuml. "Thermal Model and Behavior of a Totally-Enclosed-Water-Cooled Squirrel-Cage Induction Machine for Traction Applications". In: *IEEE Transactions on Industrial Electronics* 55 (2008), pp. 3555–3565. URL: <https://api.semanticscholar.org/CorpusID:43269809>.
- [19] Feng Chai et al. "Temperature Field Accurate Modeling and Cooling Performance Evaluation of Direct-Drive Outer-Rotor Air-Cooling In-Wheel Motor". In: *Energies* 9 (Oct. 2016), p. 818. DOI: 10.3390/en9100818.
- [20] David G. Dorrell et al. "A Review of the Design Issues and Techniques for Radial-Flux Brushless Surface and Internal Rare-Earth Permanent-Magnet Motors". In: *IEEE Transactions on Industrial Electronics* 58.9 (2011), pp. 3741–3757. DOI: 10.1109/TIE.2010.2089940.
- [21] Ping Zheng et al. "Research on the Cooling System of a 4QT Prototype Machine Used for HEV". In: *IEEE Transactions on Energy Conversion* 23.1 (2008), pp. 61–67. DOI: 10.1109/TEC.2007.914356.
- [22] Banti Khan, Ashita Goyal, and Ashutosh Kumar Chobey. "IMPROVING THERMAL WITHSTANDING CAPACITY OF THREE PHASE INDUCTION MOTOR USING NWCC METHOD". In: *International Journal of Research -GRANTHAALAYAH* 2.3 (Dec. 2014), pp. 40–51. DOI: 10.29121/granthaalayah.v2.i3.2014.3058. URL: [https://www.granthaalayahpublication.org/journals/granthaalayah/article/view/IJRG14\\_A12\\_54](https://www.granthaalayahpublication.org/journals/granthaalayah/article/view/IJRG14_A12_54).
- [23] P. Murugan et al. "A current state of metal additive manufacturing methods: A review". In: *Materials Today: Proceedings* 59 (Dec. 2021). DOI: 10.1016/j.matpr.2021.11.503.
- [24] Akash Bhatia and Anuj Kumar Sehgal. "Additive manufacturing materials, methods and applications: A review". In: *Materials Today: Proceedings* 81 (2023). International Virtual Conference on Sustainable Materials (IVCSM-2k20), pp. 1060–1067. ISSN: 2214-7853. DOI: <https://doi.org/10.1016/j.matpr.2021.04.379>.
- [25] Martin Sarap et al. "Utilization of Additive Manufacturing in the Thermal Design of Electrical Machines: A Review". In: *Machines* 10.4 (2022). ISSN: 2075-1702. DOI: 10.3390/machines10040251. URL: <https://www.mdpi.com/2075-1702/10/4/251>.
- [26] Jordi Delgado Sanglas, Joaquim Ciurana, and Ciro Rodriguez. "Influence of process parameters on part quality and mechanical properties for DMLS and SLM with iron-based materials". In: *The International Journal of Advanced Manufacturing Technology* 60 (May 2011). DOI: 10.1007/s00170-011-3643-5.
- [27] Sebastian Riecker et al. "Fused deposition modeling-opportunities for cheap metal AM". In: Oct. 2016.

- [28] Seyeon Hwang et al. "Thermo-mechanical Characterization of Metal/Polymer Composite Filaments and Printing Parameter Study for Fused Deposition Modeling in the 3D Printing Process". In: *Journal of Electronic Materials* 44 (Mar. 2015). DOI: 10.1007/s11664-014-3425-6.
- [29] Guang Hu et al. "Nanofillers can be used to enhance the thermal conductivity of commercially available SLA resins". In: *Procedia Manufacturing* 38 (Jan. 2019), pp. 1236–1243. DOI: 10.1016/j.promfg.2020.01.215.
- [30] Ana Vafadar et al. "Advances in Metal Additive Manufacturing: A Review of Common Processes, Industrial Applications, and Current Challenges". In: *Applied Sciences* 11.3 (2021). ISSN: 2076-3417. DOI: 10.3390/app11031213. URL: <https://www.mdpi.com/2076-3417/11/3/1213>.
- [31] Hongqi Guo et al. "Joining of carbon fiber and aluminum using ultrasonic additive manufacturing (UAM)". In: *Composite Structures* 208 (2019), pp. 180–188. ISSN: 0263-8223. DOI: <https://doi.org/10.1016/j.compstruct.2018.10.004>. URL: <https://www.sciencedirect.com/science/article/pii/S0263822318321858>.
- [32] Julio Villafuerte. "Considering Cold Spray for Additive Manufacturing". In: *Advanced Materials and Processes* 172 (May 2014), pp. 50–52. DOI: 10.31399/asm.amp.2014-05.p050.
- [33] Adrita Dass and Atieh Moridi. "State of the Art in Directed Energy Deposition: From Additive Manufacturing to Materials Design". In: *Coatings* 9 (June 2019), p. 418. DOI: 10.3390/coatings9070418.
- [34] Chloe Cunningham et al. "Invited Review Article: Strategies and Processes for High Quality Wire Arc Additive Manufacturing". In: *Additive Manufacturing* 22 (June 2018). DOI: 10.1016/j.addma.2018.06.020.
- [35] Byron Blakey-Milner et al. "Metal additive manufacturing in aerospace: A review". In: *Materials and Design* 209 (2021), p. 110008. ISSN: 0264-1275. DOI: <https://doi.org/10.1016/j.matdes.2021.110008>. URL: <https://www.sciencedirect.com/science/article/pii/S0264127521005633>.
- [36] Richard Russell et al. "Qualification and certification of metal additive manufactured hardware for aerospace applications". In: Jan. 2019, pp. 33–66. ISBN: 9780128140628. DOI: 10.1016/B978-0-12-814062-8.00003-0.
- [37] T. Kellner. "3D-Printed 'Bionic' Parts Could Revolutionize Aerospace Design". In: *GE Reports* (2017).
- [38] Kianian, Babak. *Wohlers Report 2017: 3D Printing and Additive Manufacturing State of the Industry, Annual Worldwide Progress Report : Chapters titles: The Middle East, and other countries*. eng. Tech. rep. Wohlers Associates, Inc., Apr. 2017.
- [39] Haizea González-Barrio et al. "Manufacturing Processes of Integral Blade Rotors for Turbomachinery, Processes and New Approaches". In: *Applied Sciences* 10.9 (2020). ISSN: 2076-3417. DOI: 10.3390/app10093063. URL: <https://www.mdpi.com/2076-3417/10/9/3063>.
- [40] Jose Ruiz et al. "METODOLOGÍA DE REPARACIÓN DE TURBOMÁQUINAS MEDIANTE LASER MATERIAL". In: *DYNA INGENIERIA E INDUSTRIA* 93 (Nov. 2018), pp. 643–648. DOI: 10.6036/8838.

- [41] C Int et al. "Rapid and cost-effective manufacturing of high-integrity aerospace components". In: *The International Journal of Advanced Manufacturing Technology* 27 (Jan. 2006). DOI: 10.1007/s00170-004-2251-z.
- [42] Martin Sarap et al. "Utilization of Additive Manufacturing in the Thermal Design of Electrical Machines: A Review". In: *Machines* 10.4 (2022). ISSN: 2075-1702. URL: <https://www.mdpi.com/2075-1702/10/4/251>.
- [43] Grzegorz Misiun et al. "Topology Optimization for additive manufacturing with distortion constraints". In: *Computer Methods in Applied Mechanics and Engineering* 386 (2021), p. 114095. ISSN: 0045-7825. DOI: <https://doi.org/10.1016/j.cma.2021.114095>. URL: <https://www.sciencedirect.com/science/article/pii/S0045782521004266>.
- [44] *Topology optimization for 3D printing - 3Dnatives*. <https://www.3dnatives.com/en/topology-optimisation140820184/>. Accessed on 10 of March 2024.
- [45] Andrew T. Gaynor et al. "Multiple-Material Topology Optimization of Compliant Mechanisms Created Via PolyJet Three-Dimensional Printing". In: *Journal of Manufacturing Science and Engineering* 136.6 (Oct. 2014), p. 061015. ISSN: 1087-1357. DOI: 10.1115/1.4028439. eprint: [https://asmedigitalcollection.asme.org/manufacturingscience/article-pdf/136/6/061015/6267652/manu\\_136\\_06\\_061015.pdf](https://asmedigitalcollection.asme.org/manufacturingscience/article-pdf/136/6/061015/6267652/manu_136_06_061015.pdf). URL: <https://doi.org/10.1115/1.4028439>.
- [46] Boyan S. Lazarov et al. "Experimental validation of additively manufactured optimized shapes for passive cooling". In: *Applied Energy* 226 (2018), pp. 330–339. ISSN: 0306-2619. DOI: <https://doi.org/10.1016/j.apenergy.2018.05.106>. URL: <https://www.sciencedirect.com/science/article/pii/S0306261918308237>.
- [47] Wessel W. Wits et al. "Freeform-Optimized Shapes for Natural-Convection Cooling". In: *2018 24rd International Workshop on Thermal Investigations of ICs and Systems (THERMINIC)*. 2018, pp. 1–6. DOI: 10.1109/THERMINIC.2018.8593305.
- [48] Mark Helou and Sami Kara. "Design, analysis and manufacturing of lattice structures: an overview". In: *International Journal of Computer Integrated Manufacturing* 31.3 (2018), pp. 243–261. DOI: 10.1080/0951192X.2017.1407456. URL: <https://doi.org/10.1080/0951192X.2017.1407456>.
- [49] Aleksey Kovalevsky et al. "Experimental Study of Aluminum Foams Thermal Conductivity. Prospects of Additive Manufacturing for Novel Heat Exchangers Production". In: *2020 IEEE 10th International Conference Nanomaterials: Applications and Properties (NAP)*. 2020, 02SAMA06-1-02SAMA06-6. DOI: 10.1109/NAP51477.2020.9309706.
- [50] Lei Yang et al. "Continuous graded Gyroid cellular structures fabricated by selective laser melting: Design, manufacturing and mechanical properties". In: *Materials and Design* 162 (2019), pp. 394–404. ISSN: 0264-1275. DOI: <https://doi.org/10.1016/j.matdes.2018.12.007>. URL: <https://www.sciencedirect.com/science/article/pii/S0264127518308785>.
- [51] Rafal Wrobel et al. "Design and experimental characterisation of an additively manufactured heat exchanger for the electric propulsion unit of a high-altitude solar aircraft". In: *2019 IEEE Energy Conversion Congress and Exposition (ECCE)*. IEEE. 2019, pp. 753–760.

- [52] Yu Rao, Bo Li, and Yan Feng. "Heat transfer of turbulent flow over surfaces with spherical dimples and teardrop dimples". In: *Experimental Thermal and Fluid Science* 61 (2015), pp. 201–209. ISSN: 0894-1777. DOI: <https://doi.org/10.1016/j.expthermflusci.2014.10.030>. URL: <https://www.sciencedirect.com/science/article/pii/S0894177714002829>.
- [53] *Additive Manufactured Electric Motor*. <https://ncam.the-mtc.org/case-studies/additive-manufactured-electric-motor/>. Accessed 12 of March 2024.
- [54] *European Powder Metallurgy Association (EPMA). Cooling Jacket with Internal Helix Structure*. <https://www.epma.com/spotlight-on-pm/cooling-jacket-with-internal-helix-structure>. Accessed 10 of February 2024.
- [55] *EV Cooling: Optimize your battery cooling system cooling with minimal effort*. <https://www.diabatix.com/applications/ev-cooling>. Accessed 12 of March 2024.
- [56] *3D Printed Metal Cooling Jacket Boost the Formula Electric Student Team*. <https://www.eplus3d.com/3d-printed-metal-cooling-jacket-boost-the-formula-electric-student-team.html>. Accessed 12 of March 2024.
- [57] Martin Philip Bendsoe and Ole Sigmund. *Topology optimization: theory, methods, and applications*. Springer Science & Business Media, 2013.
- [58] Li-Zhi Zhang. "Conjugate Heat Transfer in Plate-Fin and Tube Heat Exchangers". In: *Conjugate Heat and Mass Transfer in Heat Mass Exchanger Ducts, Elsevier* (2013), pp. 255–274.
- [59] LORENZO CATTONI. *Multi-objective topology optimization with application to MSFR*. 2020. URL: <https://hdl.handle.net/10589/174083>.
- [60] *Design Rules for Additive Manufacturing: A Categorization*. Vol. Volume 1: 37th Computers and Information in Engineering Conference. International Design Engineering Technical Conferences and Computers and Information in Engineering Conference. Aug. 2017, V001T02A035. DOI: 10.1115/DETC2017-68446. eprint: <https://asmedigitalcollection.asme.org/IDETC-CIE/proceedings-pdf/IDETC-CIE2017/58110/V001T02A035/2473303/v001t02a035-detc2017-68446.pdf>. URL: <https://doi.org/10.1115/DETC2017-68446>.
- [61] Xueye Chen. "Topology optimization of microfluidics — A review". In: *Microchemical Journal* 127 (2016), pp. 52–61. ISSN: 0026-265X. DOI: <https://doi.org/10.1016/j.microc.2016.02.005>. URL: <https://www.sciencedirect.com/science/article/pii/S0026265X16000266>.
- [62] Joe Alexandersen and Casper Schousboe Andreasen. "A Review of Topology Optimisation for Fluid-Based Problems". In: *Fluids* 5.1 (2020). ISSN: 2311-5521. DOI: 10.3390/fluids5010029. URL: <https://www.mdpi.com/2311-5521/5/1/29>.
- [63] NP van Dijk, M Langelaar, and F van Keulen. "Critical study of design parameterization in topology optimization; The influence of design parameterization on local minima". English. In: *Proceedings of the 2nd International Conference on Engineering Optimization*. Ed. by Rodrigues, H., Herskovits, J., and Mota Soares, C. 2nd International Conference on Engineering Optimization, Lisbon, Portugal ; Conference date: 06-09-2010 Through 09-09-2010. s.n., 2010, pp. 1–11. ISBN: 978-989-96264-3-0.

- [64] Martin P Bendsøe. "Optimal shape design as a material distribution problem". In: *Structural optimization* 1 (1989), pp. 193–202.
- [65] Miguel A Salazar De Troya, Daniel A Tortorelli, and Victor A Beck. "Two dimensional topology optimization of heat exchangers with the density and level-set methods". In: *WCCM-ECCOMAS Congress*. Vol. 1300. LLNL-JRNL-816310. Lawrence Livermore National Lab.(LLNL), Livermore, CA (United States). 2021.
- [66] Nico P Van Dijk et al. "Level-set methods for structural topology optimization: a review". In: *Structural and Multidisciplinary Optimization* 48 (2013), pp. 437–472.
- [67] Hyunkyoo Moon et al. "Heat transfer enhancement of single-phase internal flows using shape optimization and additively manufactured flow structures". In: *International Journal of Heat and Mass Transfer* 177 (2021), p. 121510.
- [68] Pooya Rostami and Javad Marzbanrad. "Cooperative coevolutionary topology optimization using moving morphable components". In: *Engineering Optimization* 53.6 (2021), pp. 962–983.
- [69] Gouri Dhatt, Emmanuel Lefrançois, and Gilbert Touzot. *Finite element method*. John Wiley & Sons, 2012.
- [70] Ercan M Dede. "Multiphysics topology optimization of heat transfer and fluid flow systems". In: *proceedings of the COMSOL Users Conference*. Vol. 715. 2009.
- [71] Xi Zhao et al. "A "poor man's approach" to topology optimization of cooling channels based on a Darcy flow model". In: *International Journal of Heat and Mass Transfer* 116 (2018), pp. 1108–1123.
- [72] Robert Eymard, Thierry Gallouët, and Raphaèle Herbin. "Finite volume methods". In: *Handbook of numerical analysis* 7 (2000), pp. 713–1018.
- [73] V Subramaniam, T Dbouk, and J-L Harion. "Topology optimization of conjugate heat transfer systems: A competition between heat transfer enhancement and pressure drop reduction". In: *International Journal of Heat and Fluid Flow* 75 (2019), pp. 165–184.
- [74] Zhijian J Wang et al. "High-order CFD methods: current status and perspective". In: *International Journal for Numerical Methods in Fluids* 72.8 (2013), pp. 811–845.
- [75] Amir R Khoei. *Extended finite element method: theory and applications*. John Wiley & Sons, 2014.
- [76] Aniello Riccio et al. "Robustness of XFEM method for the simulation of cracks propagation in fracture mechanics problems". In: *American Journal of Engineering and Applied Sciences* 9.3 (2016), pp. 599–610.
- [77] Peter Coffin and Kurt Maute. "A level-set method for steady-state and transient natural convection problems". In: *Structural and Multidisciplinary Optimization* 53 (2016), pp. 1047–1067.
- [78] Yi Lin et al. "A stabilized parametric level-set XFEM topology optimization method for thermal-fluid problem". In: *International Journal for Numerical Methods in Engineering* 123.4 (2022), pp. 924–952.

- [79] Lawrence Bush and Victor Ginting. "On the application of the continuous Galerkin finite element method for conservation problems". In: *SIAM Journal on Scientific Computing* 35.6 (2013), A2953–A2975.
- [80] R Merle and J Dolbow. "Solving thermal and phase change problems with the extended finite element method". In: *Computational mechanics* 28 (2002), pp. 339–350.
- [81] AA Mohamad. *Lattice boltzmann method*. Vol. 70. Springer, 2011.
- [82] Daniel Tondeur and Eric Kvaalen. "Equipartition of entropy production. An optimality criterion for transfer and separation processes". In: *Industrial & engineering chemistry research* 26.1 (1987), pp. 50–56.
- [83] Zeng-Yuan Guo, Wen-Quan Tao, and RsK Shah. "The field synergy (coordination) principle and its applications in enhancing single phase convective heat transfer". In: *International Journal of Heat and Mass Transfer* 48.9 (2005), pp. 1797–1807.
- [84] Dominique Tarlet et al. "Entropy generation analysis of a mini heat exchanger for heat transfer intensification". In: *Experimental thermal and fluid science* 53 (2014), pp. 119–126.
- [85] Michael B Giles and Niles A Pierce. "An introduction to the adjoint approach to design". In: *Flow, turbulence and combustion* 65 (2000), pp. 393–415.
- [86] Krister Svanberg. "The method of moving asymptotes—a new method for structural optimization". In: *International journal for numerical methods in engineering* 24.2 (1987), pp. 359–373.
- [87] Jasbir Singh Arora. *Introduction to optimum design*. Elsevier, 2004.
- [88] K. Deb et al. "A fast and elitist multiobjective genetic algorithm: NSGA-II". In: *IEEE Transactions on Evolutionary Computation* 6.2 (2002), pp. 182–197. DOI: 10.1109/4235.996017.
- [89] Peter I Frazier. "Bayesian optimization". In: *Recent advances in optimization and modeling of contemporary problems*. Informs, 2018, pp. 255–278.
- [90] *Navier-Stokes Equations in COMSOL multiphysics Cyclopedia*. <https://www.comsol.com/multiphysics/navier-stokes-equations?parent=modeling-conservation-mass-energy-momentum-0402-432-302>. Accessed: 1 of April 2024.
- [91] Shaopeng Wu et al. "Design and research on high power density motor of integrated motor drive system for electric vehicles". In: *Energies* 15.10 (2022), p. 3542.
- [92] Mengyuan Li et al. "Cooling water jacket design of motorized spindle system using multi-objective topology optimization". In: *Applied Thermal Engineering* 224 (2023), p. 120112. ISSN: 1359-4311. DOI: <https://doi.org/10.1016/j.applthermaleng.2023.120112>. URL: <https://www.sciencedirect.com/science/article/pii/S1359431123001412>.